STRESS ANALYSIS OF SPUR AND BEVEL GEARS BY FEM

By

C. RANGANATH

DEPARTMENT OF MECHANICAL ENGINEERING
INDIAN INSTITUTE OF TECHNOLOGY, KANPUR
NOVEMBER, 1984

STRESS ANALYSIS OF SPUR AND BEVEL GEARS BY FEM

A Thesis Submitted
In Partial Fulfilment of the Requirements
for the Degree of
MASTER OF TECHNOLOGY

By

C. RANGANATH

to the

DEPARTMENT OF MECHANICAL ENGINEERING
INDIAN INSTITUTE OF TECHNOLOGY, KANPUR
NOVEMBER, 1984

ME-1984-M-RAN-STR

17/11/84.

CERTIFICATE

This is to certify that the work entitled, "STRESS ANALYSIS OF SPUR AND BEVEL GEARS BY FEM" has been carried out under my supervision by Mr. C. Ranganath and has not been submitted elsewhere for a degree.

Bhupinder Pal Singh.

IIT Kanpur
November 1984

Bhupinder Pal Singh
Assistant Professor
Mechanical Engineering Department
Indian Institute of Technology
Kanpur 208016

ACKNOWLEDGEMENTS

I take this opportunity to express my heartfelt gratitude towards my advisor, Dr. Bhupinder Pal Singh, for his untiring guidance in this work. I am extremely thankful for his constant encouragement and valuable criticism. He has devoted much of his valuable time for which I am gratoful.

The assistance given by the Mechanical Engineering Department and the facilities made available at the Computer Centre of the Indian Institute of Technology, Kanpur are very much appreciated.

I am thankful to Mr. Umesh Muttur, Mr. Shrikanth Naik and Mr. K.G. Shastry for the assistance given at various stages of this work.

My thanks are also due to Mr. H.K. Nathani for excellent typing of the manuscript and Mr. J.C. Varma for excellent tracings within a short time.

IIT Kanpur
November 1984

C. Ranganath

CONTENTS

LIST of FIGURES and TABLES

TABLES

Table No.

NOMENCLATURE

[A]	Smoothing matrix
a	Addendum of gear
[B]	Matrix of derivatives of shape functions with respect to global coordinates (x,y,z)
b	Face width
c	Cone distance
[D]	Material property matrix
D_p	Pitch circle diameter of gear
D_b	Base circle diameter of gear
D_1	Any convenient diameter of gear
D_{pp}	PCD of pinion
D_{pg}	PCD of gear
d	Dedendum of gear
{ε}	Strain matrix
F	Forces
{FS}	Force matrix formed by the use of unsmoothed values at gauss points for local smoothing
g(r,s,t)	Function of local coordinates (r,s,t) and is given by $[B]^T[D][B]$
g	Circular tooth thickness
I	The potential
[J]	Jacobi matrix which transforms the derivatives of local coordinates to derivatives of global coordinates
[K]	Stiffness matrix
M	Module in mm.
M_s	Module at shorter end in mm

m	Mass per unit volume
N	Shape functions for stiffness matrix generation
$\bar{N}$	Shape functions for local stress smoothing
NGP	Number of gauss points
n	Number of nodes
P	Load applied on tooth
p	Uniform load on an edge
r_f	Fillet radii
r,s,t	Local (natural) coordinates
S	Surface forces
t	Thickness
u,v,w	The displacements in X,Y,Z coordinates axes directions respectively
W_i	Weight corresponding to gauss point coordinate
x,y,z	The three coordinates of a point
Z	Number of teeth
$\sigma_x, \sigma_y, \sigma_z$	Stress components at a point
$\tau_{xy}, \tau_{yz}, \tau_{zx}$	
$\varepsilon_x, \varepsilon_y, \varepsilon_z$	Strain components at a point
$\gamma_{xy}, \gamma_{yz}, \gamma_{zx}$	
$\sigma_1, \sigma_2, \sigma_3$	Principal stresses at a point
Ω	Angular velocity in rad/sec
γ	Angle subtended at the centre by the points on profile
ϕ	Pressure angle

ϕ_h	Contact angle for the tip loading
δ_a, δ_d	Addendum and dedendum angles
α	Pitch cone angle

Subscripts

i,j,k	indices
B	body forces
s	Surface forces
g	gear
p	pinion

Superscripts

(e)	Pertaining to an element
(n)	Pertaining to nodes of the whole structure
(ne)	Pertaining to nodes of a particular element

Matrix Notations

[ ]	Symmetric matrix
{ }	Column matrix
⌊ ⌋	Row matrix

ABSTRACT

A general utility FEM program which uses isoparametric elements and can handle 2-dimensional and 3-dimensional stress analysis has been developed. The stress analysis of spur and bevel gears has been carried out using this program. Local least squares stress smoothing method has been made use of in the stress calculations at nodal points.

Detailed stress analysis has been done for spur and bevel gears. The spur gears have been studied as solid and rim gears. The effects of fillet radii are studied for both the types. The effects of rim thicknesses are also studied. The effects of centrifugal forces on root stresses have also been investigated. Detailed stress plots are given for each case.

In case of bevel gears, the effects of fillet radii have been studied for two models. The stress distributions along the fillet lengths and accross the tooth section are presented. For easier application of failure criteria, the octahedral shear stress distribution is also given. A procedure for bevel gear mesh generation is presented.

CHAPTER 1

INTRODUCTION

Gears have found universal application, wherever power is to be transmitted without slip between two shafts at constant velocity ratio. There is no limit to the power that can be transmitted. The centre distance is small as compared to other types of drives. In the involute tooth form, the line of pressure and the line of action coincide on a straight line and thus the velocity ratio does not change for changes in the centre distance. This advantage has made it universally accepted as the standard tooth form.

1-1. PREVIOUS WORK

A designer who is set about to design a gear starts his design using cantilever beam formula (Lewis equation). This formula is derived considering gear tooth as a beam of parabolic cross section having uniform strength. Only the load acting horizontally is taken into account and the bending stress is calculated. The compressive load component is not taken into consideration. The compressive stress produced by this load reduces the tensile bending stress and increases compressive bending stress. The fillet radius plays very important role in the stress analysis at the root and these are not taken into account in this formula. Jaramillo [1]

has made a statement that "if the distance of the load from the clamped edge is of the order of magnitude of plate thickness the beam solution ceases to be valid". Others have also commented upon the inadequacies of cantilever beam theory for low beam heights. However in the absence of alternative approaches, the Lewis equation is still being used for prediction of stress taking suitable semiemperical stress concentration factors. The bending stress alone is not sufficient to predict failure. In these design calculations he uses a factor of safety to take care of uncertainty of stress calculations. So how high a factor of safety should be used? Too high a factor renders the design uneconomical. Another disadvantage is that displacements cannot be calculated accurately for different points on the profile.

Once the design is complete he is faced with questions like -

- Can cantilever beam theory correctly predict the two and three dimensional stresses actually occuring in the gears?
- What are the actual stresses induced and how do they compare with the assumed safe stresses?
- What is the stress range at a point?
- What are the displacements of various points on the profile, so as to take care of noise by geometrical compensation.

- What is the critical section and what are the stresses that cause failure?

The designer uses one of the following alternatives to get answersto the above questions.

(1) Experimental Methods

[i] Electrical resistance or semi-conductor strain gauge measurement

[ii] Photoelastic method

(2) Analytical Methods

(3) Numerical Methods like finite element method.

Electric strain gauges measure the strain at the chosen points. These gauges are difficult to use in the fillet regions. Lot of experimental skill and good instruments are needed to get reliable results. As this method is not a whole field method, results are of limited use only.

In photoelastic method, first a model is made of transparent material. The stresses are calculated from isochromatic and isoclinic fringe patterns. Two dimensional photoelastic analysis is quite simple and straight forward, whereas three dimensional photoelastic analysis requires stress freezing. This makes the method very involved. Detailed post analysis of slices requires experimental skills of very high order.

In analytical methods conformal mapping technique is used to represent the gear profile. The selection of

transform function needs considerable experience. This analysis is quite involved as one has to try different functions to fit the profile. The application of this method to three dimensional analysis looks almost impossible.

In the finite element method, the structural idealization of a continuum is accomplished by dividing it into number of parts called finite elements. A solution over the finite element is assumed initially in the form of a polynomial without any consideration to the boundary conditions of the structure. Using this and the variational statement or differential equation of the problem, the typical finite element equations (element stiffness, displacement and load matrices) are formed. Global equations are formed by adding the elemental matrices. Now applying the boundary conditions the displacements, strains and stresses are found at different points. This numerical technique is finding larger acceptance because of this advantage. These results have proved very reliable and are in excellent agreement with the theoretical exact solutions.

All the above techniques are being used in gear tooth stress analysis. Baronet and Tordion [2] analysed the standard tooth form using conformal mapping techniques using 2D elasticity and appropriate transform function, the stress distribution and geometry factors were found out.

Wallace and Sieveg [3] have done dynamic analysis using FEM. The analysis uses viscoelastic model to describe material behaviour for impulsive loading.

Wilcox and Coleman [4] applied FEM to symmetric and unsymmetric tooth profiles. They compared their results with photoelastic results and they were found to be in excellent agreement. They also devoloped a concentration factor that takes care of the fillet radius. The stresses calculated inside one element were averaged over 10 elements. Statistical curve fitting was used to extrapolate the stress gradient to the surface.

Chabert, Dangtran and Mathis [5] conducted study on gear tooth boundary conditions. They concluded that region bounded by the lines drawn radially between the adjacent teeth on the root circle and 1.5-2.0M below the root circle will be enough to represent the solid gear for FEM analysis. For the worst loading condition when one pair is in contact they analysed and plotted the stresses.

Oda, Nagamura and Aoki [6] studied the effects of rim thicknesses on stresses. They also concluded that one tooth model is sufficient for the analysis. The results were verified by experimental means also.

Arai , Harada and Aida [7] studied the thin rim effect on a 9 tooth model. The stress plots are given when different teeth are loaded. Again the results are compared with

experimental results.

Al-Shareedah and Lehnoff [9] have analysed straight bevel gear tooth modelling it as a plate. They compared these results with the results of finite element method. But their model is of questionable value. The profile of tooth is nowhere near the involute form. The fillets have been totally ignored.

Chang, Huston & Coy [8] have used SAP-IV to analyse both solid and thin rim gears. They have studied the effects of rim thickness, fillet radii and loading position on both these gears. The stress plots are also given.

1-2. PRESENT WORK

Most of the previous work done in stress analysis of gears by FEM has been on spur gears mostly using triangular elements In order to take care of the involute profile effectively,more number of elements have been used. The more number of elements mean more time and pain to prepare the data. It is established now that hipher order elements give same accuracy with fewer elements. It is logical to think that isoparametric elements are more suited to take care of the gear tooth profile. So it was decided that the analysis of tooth should be done using 8 node isoparametric element in 2-dimensional analysis and 20 node isoparametric element in 3-dimensional analysis.

Chang, Huston et. al [8] have studied the effects of thin rims for two rim radii. In this study the centrifugal forces were ignored. It was decided to investigate this aspect and the effects of fillet radii on thin rim gears.

The bevel gear tooth is subjected to loads in all three coordinate axes directions, when a single pair is in contact. This particular aspect brings doubts in the stress calculated by the cantilever beam (Lewis) formula. The available formulae are unable to handle this type of loading. Again a factor of safety is taken to eliminate the uncertainty. It is logical to think that at worst moment of loading, the shorter end is more severly stressed. So what is the state of stress at this end? What are stress variations along the length of the tooth? As in spur gears the fillet radii affect the stresses considerably in bevel gears also. So it was decided to do three dimensional stress analysis of bevel gears using 20 node isoparametric brick element to get a true picture of stresses.

CHAPTER II

FORMULATION

Finite element method is used for the analysis of all gear models in this work. First the finite element method for 3-dimensional analysis is explained briefly. Details are available in standard texts [10, 11, 12, 16]. One with prior knowledge of FEM may skip this portion of present chapter. The stress calculations at the node points which are not dealt in detail in other texts, are given in detail in Section 2-1.3. Mesh generation for bevel gears is explained in Section 2-2.

2-1. FINITE ELEMENT METHOD FOR 3-DIMENSIONAL ANALYSIS

Potential to be minimized is

$$I = \int_V \frac{1}{2} \sigma \varepsilon dv - \int_V F_i u_i dv - \int_s S_i u_i ds \qquad (1)$$

Here the first term represents the strain energy, the second term represents the work done by body forces and the third term represents the work done by surface forces. The strain and stress matrices are

$$\lfloor \varepsilon \rfloor = \lfloor \varepsilon_x, \varepsilon_y, \varepsilon_z, \gamma_{xy}, \gamma_{yz}, \gamma_{zx} \rfloor \qquad (2)$$

$$= \left\lfloor \frac{\partial u}{\partial x}, \frac{\partial v}{\partial y}, \frac{\partial w}{\partial z}, \frac{\partial u}{\partial y} + \frac{\partial v}{\partial x}, \frac{\partial v}{\partial z} + \frac{\partial w}{\partial y}, \frac{\partial w}{\partial x} + \frac{\partial x}{\partial z} \right\rfloor$$

$$\lfloor \sigma \rfloor = \lfloor \sigma_x, \sigma_y, \sigma_z, \tau_{xy}, \tau_{yz}, \tau_{zx} \rfloor \qquad (3)$$

Strain and stress matrices are related by [D] matrix as

$$\{\sigma\} = [D]\{\varepsilon\} \tag{4}$$

Displacements over the finite element are taken as

$$\begin{Bmatrix} u \\ v \\ w \end{Bmatrix}^{(e)} = \begin{bmatrix} |N| & |0| & |0| \\ |0| & |N| & |0| \\ |0| & |0| & |N| \end{bmatrix} \begin{Bmatrix} u \\ v \\ w \end{Bmatrix}^{(ne)} \equiv [N]\{u\}^{(ne)} \tag{5}$$

where N are the shape functions.

Using (5), strain matrix equation (2) becomes

$$\{\varepsilon\} = [B]\{u\}^{(ne)} \equiv [B]_i \begin{Bmatrix} u \\ v \\ w \end{Bmatrix}_i \tag{6}$$

where

$$[B]_i = \begin{bmatrix} N_{i,x} & 0 & 0 \\ 0 & N_{i,y} & 0 \\ 0 & 0 & N_{i,z} \\ N_{i,y} & N_{i,x} & 0 \\ 0 & N_{i,z} & N_{i,y} \\ N_{i,z} & 0 & N_{i,x} \end{bmatrix}$$

Substituting the equations (4), (5) and (6) in equation (1) one gets

$$I^{(e)} = \frac{1}{2} \lfloor u \rfloor^{ne} \int_V [B]^T [D][B]\, dv\, \{u\}^{ne} - \lfloor u \rfloor^{ne} \int_V F[N]^T dv - \lfloor u \rfloor^{ne} \int_B p[N]^T ds \tag{7}$$

By applying the Rayleigh Ritz method, one gets

$$[K]^e \{u\}^{(ne)} = \{F_B\}^{(e)} + \{F_S\}^{(e)} \tag{8}$$

Here

$$[K]^{(e)} = \int_v [B]^T[D][B]dv \tag{9}$$

$$\{F_B\}^{(e)} = \int_v F [N]^T dv \tag{10}$$

$$\{F_S\}^{(e)} = \int_A p[N]^T ds \tag{11}$$

where $[K]^{(e)}$ is the elemental stiffness matrix, $\{F_B\}^{(e)}$ is the body force matrix and $\{F_S\}^{(e)}$ is the surface force matrix. Elemental equilibrium Equations (8) are added up to obtain global equilibrium equations of the form

$$[K] \{u\}^{(n)} = \{F\}^{(n)} \tag{12}$$

where [K] is the global stiffness matrix, $\{u\}^{(n)}$ is the overall displacement matrix and $\{F\}^{(n)}$ is the global force matrix. The displacements are found by solving these simultaneous equations after applying the boundary conditions.

The stresses and strains are calculated by the use of Equations (6) and (4).

2-1.1 Isoparametric elements and numerical integration

First the finite element with curved boundaries is mapped into a cube of side 2 using

$$x = \sum_{i=1}^{\text{nodes}} N_i x_i, \quad y = \sum_{i=1}^{\text{nodes}} N_i y_i, \quad z = \sum_{i=1}^{\text{nodes}} N_i z_i \tag{13}$$

Here shape functions N_i may be same or different from those used for dependent variables u,v,w in Equation (5). If these shape functions are same as those in Equation (5), the finite element is known as isoparametric element and has been used in this work. These shape functions are expressed in natural (local) coordinates (r,s,t). Using Equation (13), the elemental stiffness matrix Equation (9) becomes

$$[K]^{(e)} = \iiint_{V^{(e)}} [B]^T[D][B]\, dx\,dy\,dz = \int_{-1}^{1}\int_{-1}^{1}\int_{-1}^{1} [B]^T[D][B]\, \det[J]\, dr\, ds\, dt \qquad (14)$$

Here [B] matrix is evaluated using the Jacobi matrix [J], see Ref. [10,11,12,16]. Jacobi matrix [J] transforms the local coordinate derivatives into global coordinate derivatives. Using Gauss-Legendre quadrature formula, the above stiffness matrix is evaluated as follows

$$[K]^{(e)} = \sum_{i=1}^{NGP}\sum_{j=1}^{NGP}\sum_{k=1}^{NGP} W_i W_j W_k g(r_i,s_j,t_k) \det [J] \qquad (15)$$

where $g = [B]^T[D][B]$ is evaluated at the various gauss points and $W_i W_j W_k$ are the weights corresponding to the Gauss point (r_i,s_j,t_k). These values are taken from the gaussian quadrature table [10,11,16]. The number of gauss points chosen depends on the order of polynomials to be integrated. Thus for 3-dimensional brick element with 20 nodes the order of polynomial is six and four gauss points are needed in each direction for its accurate determination. But it has been

found that three gauss point integration is accurate enough [10], and has been used.

2-1.2 Centrifugal Load Matrix

For two-dimensional problems, this body force matrix becomes

$$\{F_B\}^{(e)} = \int\int \Omega^2 m \, [N]^T \begin{Bmatrix} x \\ y \end{Bmatrix} t\,dx\,dy \qquad (16)$$

Here m is the mass per unit volume; Ω is the angular velocity, $\begin{Bmatrix} x \\ y \end{Bmatrix}$ is the radius vector from the axis of rotation and t is the thickness. Equation (16) after it is mapped into a square of side 2 becomes

$$\{F_B\}^{(e)} = \int_{-1}^{1}\int_{-1}^{1} \Omega^2 m \, [N]^T \begin{Bmatrix} x \\ y \end{Bmatrix} \det[J] \, t\,dr\,ds \qquad (17)$$

This force matrix is evaluated by using Gauss-Legendre quadrature formula as explained in Section 2-1.1. In this matrix $\begin{Bmatrix} x \\ y \end{Bmatrix}$ is evaluated at the gauss points using Equation (13).

2-1.3 Stress Evaluation

The global stiffness matrix is assembled as a profile matrix. The system of simultaneous equations is solved by gaussian elimination. From displacements the stresses at any point (r_i, s_i, t_i), $\{\sigma\}^{(e)}$, is calculated by

$$\{\sigma\}^{(e)} = [D] \, [B(r_i, s_i, t_i)] \, \{u\}^{(ne)} \qquad (18)$$

Here $\{u\}^{(ne)}$ represents the displacement vector for that particular

element. But it is well established that the stresses calculated at nodal points straightaway will be in considerable error. Experience [10] has shown that the gauss points are the best sampling points for stresses. Since nodes are most useful output locations for stresses, a need was felt for extrapolation of gauss point stresses to the nodes in each element by local smoothing [13,14]. Essentially in this procedure the nodal values are found by an exact least square fit to the unsmcothcd values at the gauss pcints. The procedure which is carried out for each element is given by [13,14]

$$\begin{bmatrix} \sum_{i=1}^{NGP} \bar{N}_1(r_i,s_i,t_i)\bar{N}_1(r_i,s_i,t_i) & \cdots & \sum_{i=1}^{NGP} \bar{N}_1(r_i,s_i,t_i)\bar{N}_n(r_i,s_i,t_i) \\ \vdots & & \\ \sum_{i=1}^{NGP} \bar{N}_n(r_i,s_i,t_i)\bar{N}_1(r_i,s_i,t_i) & \cdots & \sum_{i=1}^{NGP} \bar{N}_n(r_i,s_i,t_i)\bar{N}_n(r_i,s_i,t_i) \end{bmatrix}$$

$$\begin{Bmatrix} \sigma_1 \\ \sigma_2 \\ \vdots \\ \sigma_n \end{Bmatrix} = \begin{Bmatrix} \sum_{i=1}^{NGP} \bar{N}_1(r_i,s_i,t_i)\sigma_i \\ \vdots \\ \sum_{i=1}^{NGP} \bar{N}_n(r_i,s_i,t_i)\sigma_i \end{Bmatrix} \qquad (19)$$

$$\text{or } [A] \quad \{\sigma\}^{(nc)} = \{FS\} \tag{20}$$

Here the matrix [A] is the smoothing matrix. In the formation of this matrix shape functions $\lfloor N \rfloor$ are one order less (i.e. linear functions for quadratic elements) than those used for stiffness matrix formation. The right hand side matrix {FS} is the force matrix formed by the use of unsmoothed values of stresses at different gauss points. $\lfloor \sigma_1, \sigma_2, \ldots, \sigma_n \rfloor$ are the smoothed nodal stress values at the corner nodes of this element. Here NGP is the total number of gauss points used in the stiffness matrix formation. This procedure is repeated for all the elements, At each node average is taken of all stresses given by different elements connected at that node. The midside node stresses are calculated by taking the average of stresses at the adjacent nodes.

2-2. BEVEL GEAR MESH GENERATION

A diagramatic illustration of the bevel gear model is shown in Figure 2-1. For the convenience of construction the face of the shorter end is taken as parallel to XZ plane. The coordinate axes are also shown. As shown in Figure 2-2 the line PQO passes through apex and pitch points of both ends. The plane which contains this line is parallel to xy plane. Firstly the front view is constructed. Then the side and lastly the top views are constructed.

Construction of front view: The terminology is indicated in Figure 2-3. For a typical involute profile, the angle subtended at the centre by the points A and B on the pitch circle, (γ), is given by [17] as

$$\gamma = g/D_p \tag{21}$$

Here D_p is the P.C.D and g is the circular tooth thickness and is given by

$$g = \frac{1}{2} \times \pi \times M \tag{22}$$

The distance AB on the pitch circle = $\gamma \times D_p/2$

The angle γ_o subtended at the centre by the points C and D on the base circle (D_b) is given by [17]

$$\gamma_0 = \gamma + \text{inv}\phi \tag{23}$$

Here inv is the involute function and is given by [17]

$$\text{inv}\phi = \tan\phi - \phi \tag{24}$$

where ϕ is the pressure angle in radians.

The distance CD on the base circle = $\gamma_o \times D_b/2$. Take any convenient diameter D_1. If this is the pitch circle diameter the pressure angle is given by

$$\phi_1 = \cos^{-1} \left(\frac{D_b}{D_1}\right) \tag{25}$$

The angle γ_1 subtended at the centre by the points E and F on the circle D_1 is given by

$$\gamma_1 = \gamma_0 - \text{inv}\ \phi_1 \tag{26}$$

Using Equation (24) $\text{inv}\phi_1$ is calculated.

The distance EF on the circle (D_1) is $\gamma_1 \times D_1/2$.

Take few more convenient diameters on the profile and calculate the distances on these circles. Measure off these distances on both the sides of the axis of symmetry. Complete the profile by joining all these points. With suitable fillet radius draw the curve such that it is just touching root circle and the profile. Construct a region bounded by a distance 2M and the points on the root circle midway between the adjacent teeth. Using this procedure the profiles of bigger and shorter ends are constructed by taking the respective backcone radius as pitch circle radius [18].

Construction of side and top views: The line PQO is taken as the horizontal axis. On this line first the point P is fixed. On the perpendicular drawn at this point mark off addendum and dedendum of the bigger end. Point Q is fixed after measuring horizontally . . the face width on PQO. Measure off addendum and dedendum of shorter end on the perpendicular drawn at this point. A section XX' which is 2M distance below the root circles at both ends fixes the lower surface of the model. Intermediate lines on which the Z coordinates are measured, are drawn depending upon the lengthwise sections of the tooth. With the help of front and side views construct top view.

Construct the FEM meshes on shorter and bigger ends taking into consideration the fillet regions. The corresponding end points of any line on the shorter and bigger ends are transferred from the front view to the other two views. The X-coordinates and Y-coordinates of all the points lying on this line, are measured from the top view. Similarly the Z coordinates of the points lying on this line are measured from the side view. The uniform load is distributed to different nodes on the line RS. Depending upon the angle made by line RS in top and side views these loads are resolved in all the three coordinate axes directions.

CHAPTER III

RESULTS AND DISCUSSIONS

As said earlier spur gears (solid and rim) and bevel gears have been studied and results are given in this chapter. For spur gears, two models SG90 and SG270 having pitch diameters of 90 and 270mm respectively were chosen. These gears were modelled as plane stress problems. Effects of fillet radii on stress distribution were studied on solid and rim gears. Rim gears of different thickness were also studied. Effect of speed was studied in thin rim gears. Spur gear SG90 was also investigated as 3-dimensional body. Next two bevel gears BG100 and BG180 having pitch diameters of 100 and 180mm respectively were studied. These gears were modelled as 3-dimensional bodies. Effects of fillet radii on stress distribution were studied.

For two-dimensional analysis eight node isoparameteric quadrilateral elements and for three-dimensional analysis twenty node isoparametric brick elements were used. For eight node quadrilateral elements two gauss points and for twenty node brick elements three gauss points were used in each direction for numerical integration.

Fillet region of the loaded side has been called +ve fillet side and the other one as -ve fillet side in the present study.

3-1. STUDY OF SPUR GEAR, SG-90

This spur gear was studied by [8] and was chosen here to check the validity of the prestent computer programme. It may be noted that Ref. [8] used triangular elements with three nodes, whereas the present study uses eight noded isoparametric quadrilateral elements. In the present study gear was divided into 28 elements with 111 nodes, see Fig. 3-1.(a) Specifications of this gear are as follow:

Number of teeth, Z	= 18
Module, M	= 5mm
Pcd of gear, D_p	= 90mm
Addendum, a = 1M	= 5mm
Dedendum, d = 1.25M	= 6.25mm
Load applied, P	= 400 kN/m
The angle of contact at the top, ϕ_t	= 30° 17'
The fillet radii studied, r_f	= 0.2M,0.3M,0.4M,0.5M

3-1.1 Comparison with Earlier Results

The model SG90 was analysed for tip loading. The rim thickness was 0.75M. Figure 3-2 shows the plots of stresses obtained from the program. These results are in good agreement with the stresses plotted by Chang et al [8] for the same.

Principal stress σ_1 is maximum on the +ve fillet side and negligible on the -ve fillet side. Similarly σ_2 is maximum on the -ve fillet side and negligible on the +ve fillet side. The compressive principal stress σ_2 is about 35% more than the tensile principal stress σ_1. Understandably the maximum shear stress occurs on the -ve fillet side. The stress gradients are very high near the surface of the tooth.

3-1.2 Effects of Fillet Radii

Figure 3-3 shows the stresses across the tooth section for different radii 0.2M to 0.5M. Increase in fillet radii reduces the fillet stresses as expected. Increase of radii from 0.2M to 0.5M reduces the principal stresses approximately by 35%. The max shear stress occurs on the -ve fillet side and this reduces approximately by 25% when radii changes from 0.2M to 0.5M.

3-2. STUDY OF SPUR GEAR, SG 270

This gear has PCD Of 270mm. This gear was studied as solid and rim gear with different rim thicknesses. Effects of fillet radii and speed were studied on thin rim gears. Specifications of this gear are as follow

Number of teeth, Z	= 54
Module, M	= 5mm
PCD of gear, D_p	= 270mm
Addendum, 1M (a)	= 5.0mm
Dedendum, 1.25M (d)	= 6.25mm
Load applied, P	= 400 kN/m
The angle of contact at the top, ϕ_h	= 25° 1'
Fillet radii studied, r_f	= 0.2M,0.3,0.4M,0.5M

3-2.1 As Solid Gear

Solid gear is modelled as shown in Figure 3-1(b) only one tooth is taken, and a portion of radial thickness of 2M below the root circle is included in the tooth for stress analysis [5,6]. Stress variation across the tooth thickness for different fillet radii is shown in Figure 3-4. Principal stresses reduce approximately by 20% when fillet radii changes from 0.2M to 0.5M. It is observed that the fillet radius has little effect on internal stress distribution.

3-2.2 The Effects of Rim Thicknesses

Results obtained for this model SG270 are tabulated in Table 1. The rim thickness is varied from .5M to 3M. The predominant principal stresses on +ve and -ve fillet sides are taken for comparison. The variation of stresses is negligible when rim thickness increases 1.5M to 3M. The stresses of 3.0M are taken as the base stresses for comparison. When the rim thickness reduces to 1.0M there is a rise of about 15% for σ_2 and τ_{max}. Least rim thickness of 0.5M produces almost 80% rise in these stresses. The compressive stresses increase much more rapidly than the tensile stresses. This observation is found to be in agreement with the findings of Chang et. al [8].

3-2.2 Effects of Fillet Radii

For this model rim thickness was taken as 1.0M and stress plot is given in Figure 3-5. Stresses at the fillets decrease

with increase in fillet radii. The internal stress distribution is not affected appreciably by the increase in fillet radii. The stresses at the fillets reduce approximately by 25% when fillet radius changes from 0.2M to 0.5M. As expected the max shear stress occurs on the -ve fillet side.

3-2.4 The Effects of Centrifugal Forces

Model SG270 was analysed for 2 different speeds of 600 and 6000 rpm. The predominant stresses are tabulated in Table 2. The effects at 600 rpm are negligible. Therefore, the results as obtained for the speed of 6000 rpm are only tabulated. It is seen that even for this speed, change in stresses is small, of the order of 1 to 3%. Because the centrifugal forces are always positive, the compressive fillet stress is reduced, while the tensile fillet stress is increased.

3-3. ANALYSIS OF SPUR GEAR AS THREE DIMENSIONAL BODY

Spur gear SG00 was analysed as three dimensional body using 20 node isoparametric brick elements. Model had 36 elements with 286 nodes. Specifications of this gear are the same as those given in Section 3-1.

The predominant principal stresses are plotted in Figure 3-6(a) and Figure 3-6(b) for +ve fillet and -ve fillet lengths respectively. The 2D value is also plotted on the graph. It is interesting to note that the stress value of 3D analysis approaches the value obtained by 2D analysis at the middle of the tooth. The stresses decrease towards either end of the tooth. This is

because the points at the two ends are free to move in all the directions. The peak values occur in the middle region of the tooth length. Since these peak values obtained by 3-D analysis are about 3% more than the 2D values, it is on the safer side to analyse the spur gears for uniform load along the length of the tooth by 2D analysis.

3-4. STUDY OF BEVEL GEARS

Two Bevel gear models BG100 and BG180 having pitch diameters of 100 and 180mm respectively were analysed. The details of these models are in the corresponding sections. Each model was analysed for four fillet radii. As said earlier the stresses of each node were calculated using twenty noded isoparametric elements. The principal and octahedral shear stresses across the fillet lengths, tooth sections and tooth profiles are plotted in various figures. Shorter and bigger ends are identified by SE and BE in the figures for bevel gears.

Fillet lengths along which the stress variations are plotted, were chosen as follow. For any fillet radius, the point with maximum predominant principal stress was selected on the shorter end. The lengthwise distribution is plotted along the line joining this point and the corresponding point on the bigger end of tooth.

The octahedral shear stress distribution is also plotted along this line. At each node on the profile of the shorter end a perpendicular to the profile is drawn. The corresponding principal stresses are plotted on these lines for the distribution along the profile.

3-4.1 Bevel Gear, BG100

This model was analysed for 4 fillet radii of 0, $0.2M_s$, $0.4M_s$, $0.55M_s$, where M_s is the module at the shorter end. The specifications are as given below:

Number of teeth on pinion Z_p	= 16
Number of teeth on gear Z_g	= 20
Module, M	= 5mm
Pcd of Pinion, D_{pp}	= 80mm
Pcd of Gear, D_{pg}	= 100mm
Addendum, a = 1M	= 5mm
Dedendum, d = 1.2M	= 6mm
Face width, b = 6.0M	= 30mm
The analysis is done for the gear	
The module at the shorter end, M_s	= 2.657mm
Cone distance, C	= 64.031mm
Pitch cone angle, α	= 51.34 deg
Addendum angle, δ_a	= 4.250° (deg)
Dedendum angle, δ_d	= 5.097° (deg)
Formative number of teeth Z_f	= 32
The load applied, P	= 400 kN/m

Figure 3.7(a) and Figure 3.7(b) show the variation of different stress along the -ve fillet length, and Fig. 3.8(a) and Fig. 3.8(b) show the same for the +ve fillet length. It is seen that shorter end is more severly stressed. For example the predominant principal stresses decrease approximately by 35% at the bigger end than those at the shorter end. Also all the stresses decrease with increasing fillet radii. For example the predominant principal stresses decrease approximately by 20% by increasing the fillet radius to 0.55 M_s. Bending stress σ_z also shows the similar trend. It is observed that maximum of σ_y and σ_3 occurs at about $\frac{1}{3}$ distance from the shorter end on both fillet sides.

Figure 3-9 shows the variation of stresses accross the thickness of the tooth at the shorter end. On the +ve fillet side σ_1 is predominant and σ_2 is predominant at the -ve fillet side as expected. The compressive principal stress σ_2 is more than tensile principal stress σ_1 as in spur gears. The bending stress σ_z shows linear variation across the tooth as expected by the cantilever beam theory. The fillet radius has no significant influence on the internal stress distribution as in spur gears.

Figure 3-10(a) shows the variation of octahedral shear stress across the tooth section. The maximum value of octahedral shear stress occurs on the -ve fillet side of the tooth and is about 40% higher than that on +ve side. By increasing the fillet radius to 0.5M this stress comes down by 20% on the -ve fillet side. It is noted that fillet radius has negligible effect on the internal stress distribution.

Figure 3.10(b) shows length wise distribution of octahedral shear stress on the -ve fillet side. The value at the bigger end is about 30% less than the value at the shorter end and the decrease is monotonic.

Figure 3-11 shows the distribution of predominant principal stresses along the profile of the tooth at the shorter end. Except for the case of zero fillet radius, the max values occur at points A and B. The values decrease on either side of these points. Thus A-B can be called as the critical section.

3-4.2 Bevel Gear, BG180

This bevel gear was analysed for 4 fillet radii of 0, $0.3M_s$, $0.4M_s$ and $0.5M_s$. Specifications of this bevel gear are as follow:

Number of teetch on pinion, Z_p	= 18
Number of teetch on gear, Z_G	= 20
Module, M	= 10mm
Pcd of pinion, D_{pp}	= 180mm
Pcd of gear, D_{pg}	= 200 mm
Addendum, a = 1M	= 10mm
Dedendum, d = 1.2M	= 12mm
Face width, b = 6M	= 60mm
The Analysis is done for the pinion.	
The module at the shorter end, M_s	= 5.54 mm
Cone distance, C	= 134.536mm
Pitch cone angle, α	= 41.987 deg
Addendum angle, δ_a	= 4.250 deg
Dedendum angle, δ_d	= 5.097 deg
Formative number of teetch, Z_f	= 24.21
The load applied, P	= 400 kN/m

Stresses obtained for this bevel gear are shown in Figure 3-12 to Figure 3-16. Study of these figures show that stress distributions are very similar to those obtained for the earlier bevel gear, BG100. They differ only in the percentage variations. Therefore results are not discussed again.

CHAPTER IV

CONCLUSIONS

From the results obtained for spur and bevel gears it is seen that cantilever bear formula (Lewis equation) cannot predict the true stresses in the fillet region and gives very inaccurate results for thin rim spur gears. From the study of 2-D analysis of spur gears, it is verified that a distance of 2M below the root circle is sufficient to analyse a solid gear. In two spur gears studied, it was found that the stresses in the fillet region decreased approximately by 20% when fillet radii increased from 0.2M to 0.5M. For thin rims, as expected, it was found that the stresses increased with decreasing rim thickness. When rim thickness decreased from 2M to 0.5M, the stresses in the fillet region increased almost by 80%. The effects of fillet radii on stress distribution are more than those in solid gears. Keeping this in view it is recommended that rim thicknesses be at least 0.75M. The centrifugal forces at 6000 rpm, when taken into account, did not affect the stresses appreciably. Hence it is justified to neglect these effects for the root stress calculations.

Three dimensional analysis of spur gears showed that the stresses in the mid region of tooth reach the 2-dimensional stress values. At both ends of tooth the stresses are lower than those at the midregion. Hence the 2-dimensional analysis of uniformly loaded spur gears is justified.

In case of bevel gears it was observed that the shorter end is much more severly stressed than the bigger end. In the two bevel gears studied, it was observed that stresses in the fillet region decreased by about 20% at the shorter end when fillet radii changed from 0.0 to 0.5"s. This decrease was less at the bigger end. The stress distribution accross the thickness were as in spur gears. The octahedral shear stress was also maximum at the shorter end.

REFERENCES

1. Jaramillo, T.J., 'Deflections and moments due to concentrated load on a cantilever plate of infinite length', Journal of applied mechanics, March 1950, pp. 67-72.

2. C.N. Baronet and G.V. Tordion, 'Exact stress distribution in standard gear teeth and geometry factors', ASME Journal of Engineering for Industry (JEFI), Vol. 95, No. 4, Nov. 73, pp. 1959-1163.

3. D.B. Walla ce & A. Seireg, 'Computer simulation of dynamic stress, deformation and fracture of gear teeth', ASME Journal of Engg for Industry (JEFI), Vol. 95, No. 4, Nov. 73, pp. 1108-1113.

4. Wilcox, L. and Coleman, W., 'Application of finite elements to the analysis of gear tooth stresses', ASME Journal of Engg for Industry, Vol. 95, No. 4, Nov. 1973, pp. 1139-1148.

5. Chabert, G., Dangtran, T and Mathis, R., 'An evaluation of stresses and deflections of spur gear teeth under strain', ASME Journal of Engg for Industry, Vol. 96, No. 1, Feb. 1974, pp. 85-93.

6. Oda, S., Nagamura, K. and Aoki, K., 'Stress analysis of thin rim spur gears by finite element method', Bull. of JSME, Vol. 24, No. 193, July 1981, pp. 1273-1280.

7. Arai , N., Harada, S., Aida Toshio, 'Research on bending strength properties of spur gears with thin rim', Bulletin of the JSME, Vol. 24, No. 195, Sept. 1981, pp. 1642-1650.

8. Chang, S.H., Huston, R.L., Coy, J.J., 'A finite element analysis of spur gears including fillet radii and rim thickness effects,' ASME Journal of Mechanisms, Transmissions and Automation in Design, Vol. 105, Sept. 1983, pp. 327-330.

9. Al-Shareedah, E.M., and Lehnhoff, T.F., 'Strength calculations for forged straight bevel gear teeth having a linking web', Int. Journal of Mech. Sciences, Vol. 26, No. 1, pp. 63-72, 1984.

10. Zienkiewicz, O.C., 'The finite element Method'(1979), Tata McGraw-Hill.

Bathe, K.J. and Wilson, E. L., 'Numerical Methods in Finite Element Analysis', (1978), Prentice-Hall of India.

Desai, C.S. & Abel, F.A., 'Introduction to FEM' (1977), East-West Press.

Hinton, E. and Campbell, J., 'Local and global smoothing of discontinuous finite element functions using a least square method', Int. J. Numerical Methods in Engg., Vol. 8, 1974, pp. 461-480.

Hinton, E., Scott, F.C. and Rickets, R.E., 'Local least squares stress smoothing for parabolic isoparametric elements', Int. Journal of Numerical Methods in Engg., Vol. 9 1975, pp. 235-256.

Chaung, Y.K. and Yeo, M.F., 'A Practical Introduction to Finite Element Analysis', (1979), Pitman Publishing Ltd.

Cook, R.D., 'Concepts and applications of finite element analysis', 2nd Ed., (1981), John Wiley.

Meritt, H.E, 'Gear Engineering', 1980, Wheeler Publications.

Maleev, V.L. and Hartman, J.B., 'Machine Design', (1983), CBS Publishers & Distributors.

Table 1

Stresses for different rim thicknesses

Stresses / Rim thicknesses	-ve fillet side σ_2	+ve fillet side σ_1	-ve fillet side τ max	% increase based on 3.0M stresses		
				σ_2	σ_1	τ max
3.0M	-362.40	296.0	140.81	0	0	0
2.0M	-367.40	294.91	143.16	1.3	-.3	1.3
1.5M	-380.97	297.69	148.13	5.1	0.5	5.2
1.0M	-423.66	314.36	164.15	17.1	6.2	16.6
0.5M	-649.61	420.57	250.75	79	42.08	78.07

Varation of stresses with Speed

Rim Thickness	Without centrifugal forces			With centrifugal forces at 6000 rpm		
	σ_1	σ_2	τ_{max}	σ_1	σ_2	τ_{max}
-ve fillet 0.5M	-148.11	-649.61	250.75	-145.51	-638.48	246.48
+ve fillet	420.57	85.57	167.5	431.48	87.82	171.83
-ve fillet 1.0M	- 95.36	-423.66	164.15	- 93.35	-417.66	161.86
+ve fillet	314.36	64.75	124.80	320.469	66.06	127.21
-ve fillet 1.5M	- 84.7	-380.97	148.13	- 83.57	-376.24	146.33
+ve fillet	297.69	60.74	118.47	302.55	61.8	120.38
-ve fillet 2.0M	- 81.09	-367 40	143.16	- 80.09	-363.24	141.7
+ve fillet	294.91	59.98	117.47	299.26	60.92	119.17

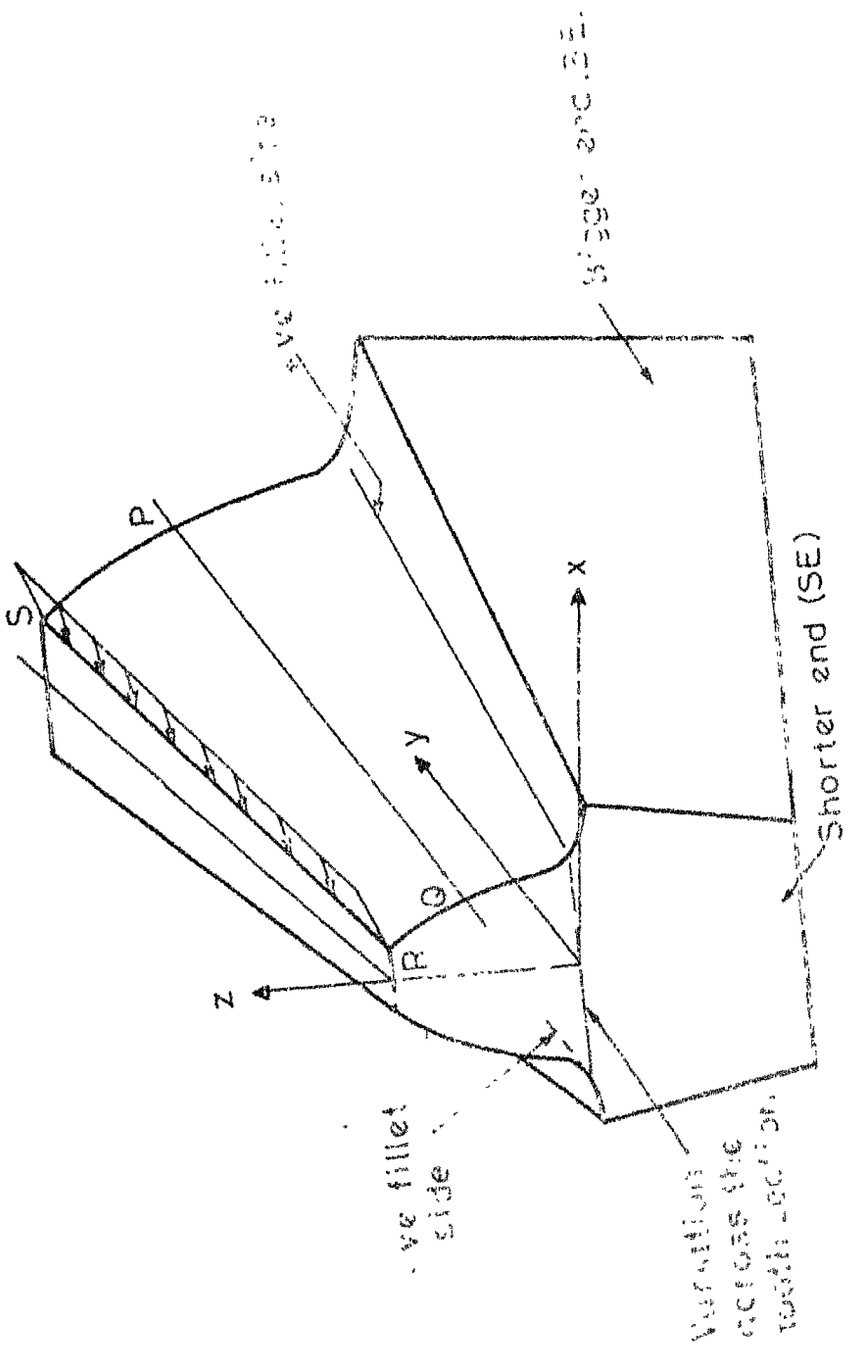

Fig. 2.1 Bevel gear

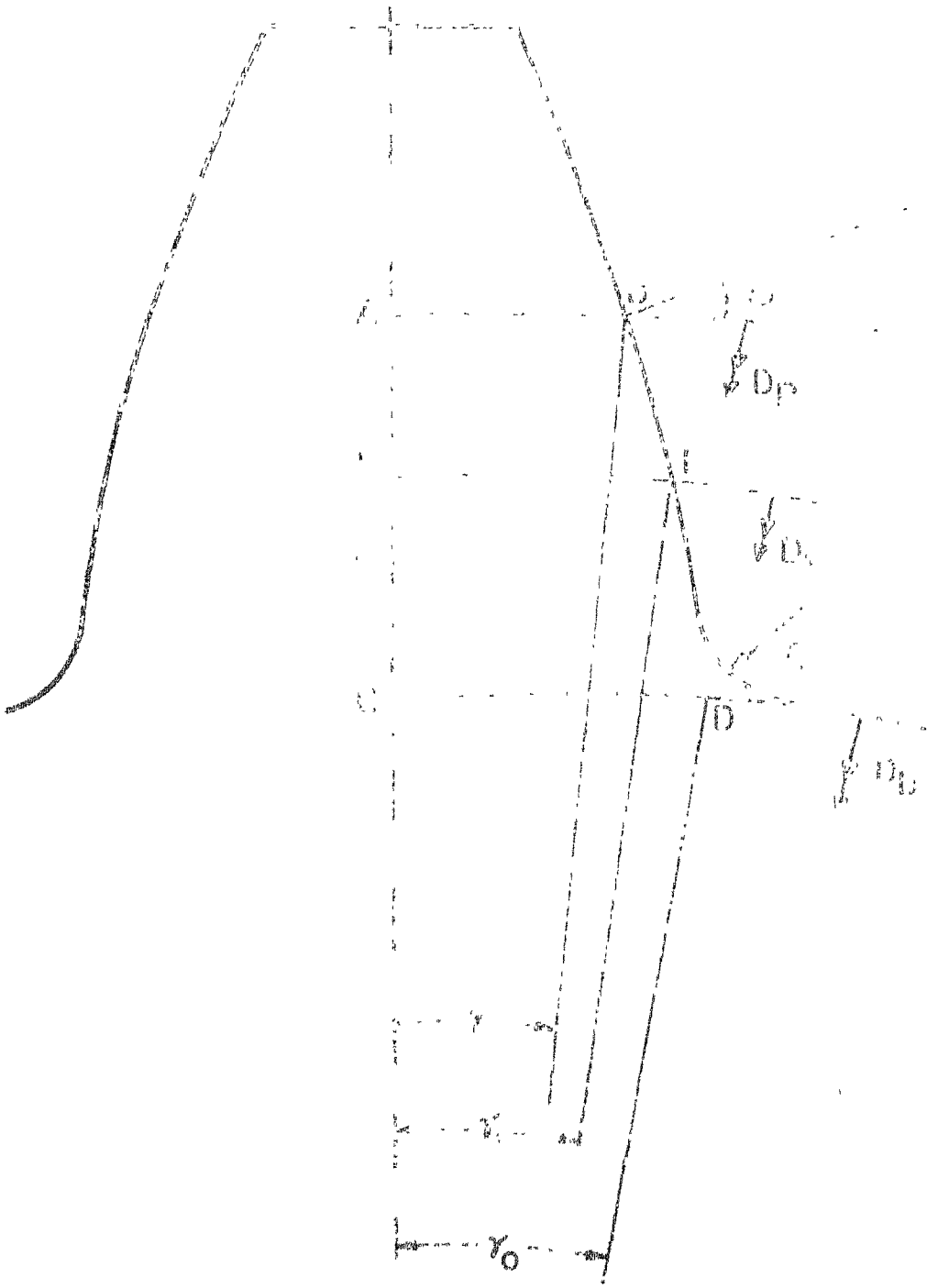

Fig.2·3 Details for the profile construction

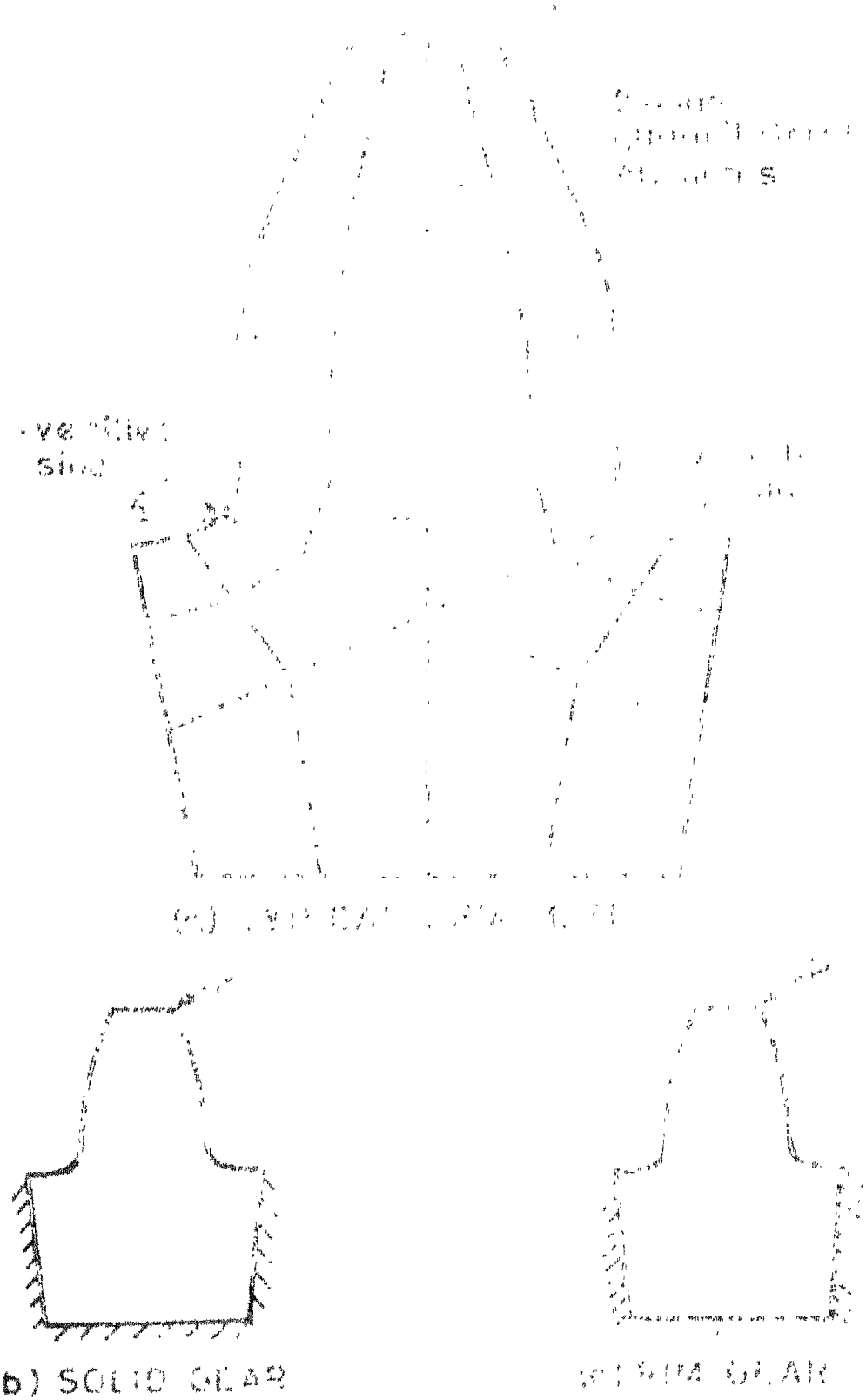

Fig.3: Spur gear models

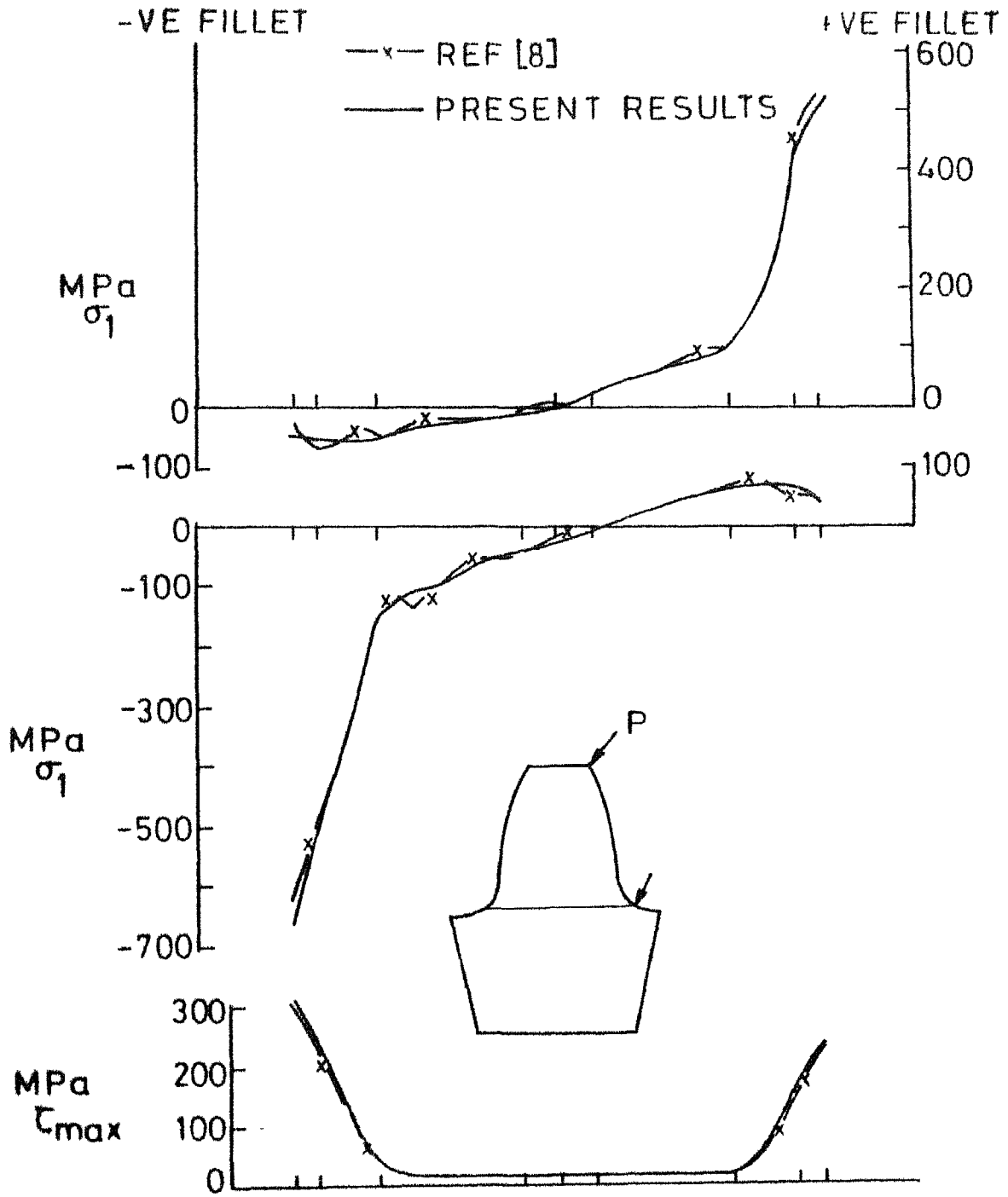

Fig.3.2 Comparison of stresses of SG 90 with Chang et. al.[8]

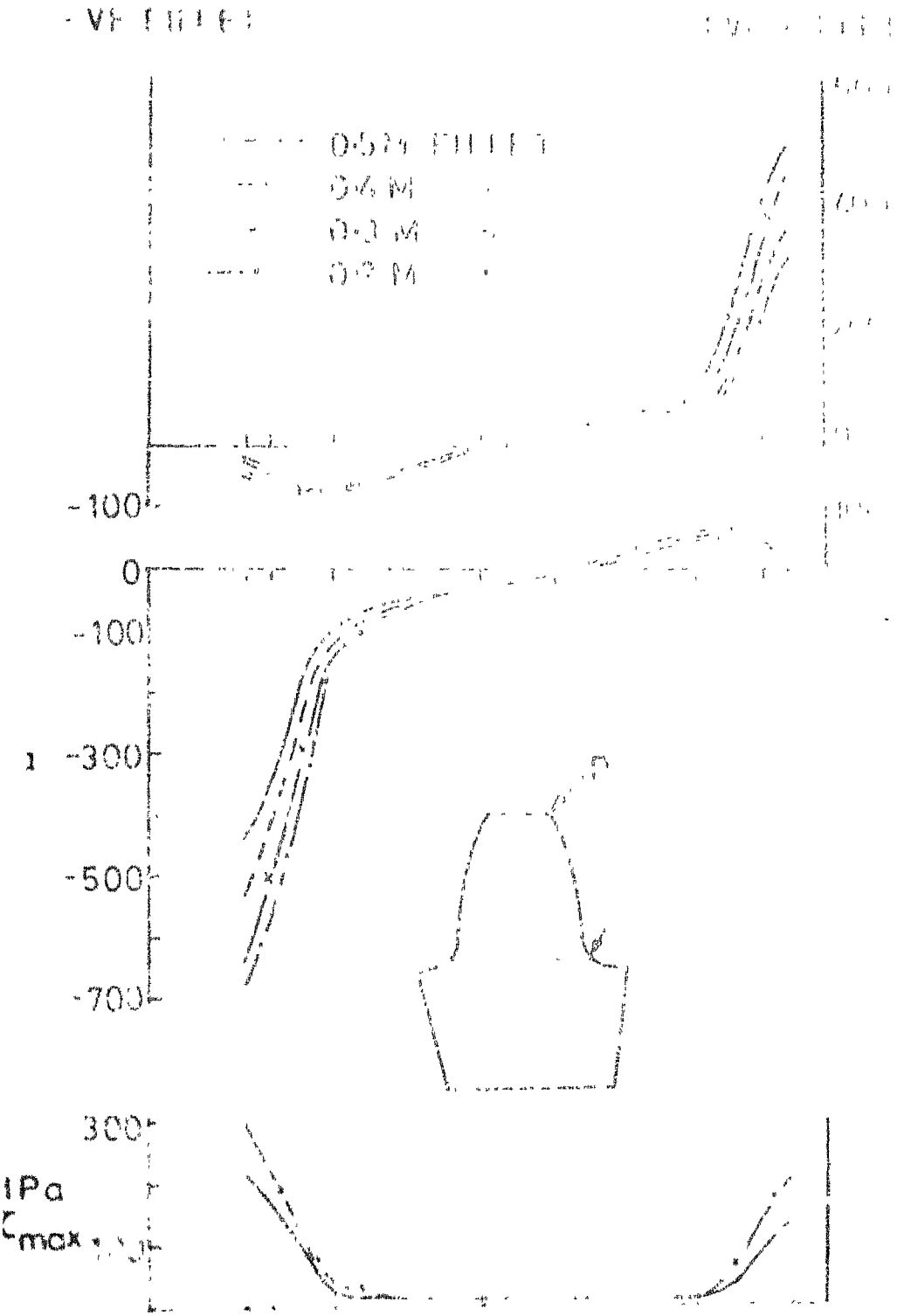

Fig.33 Stresses [illegible] section of rim gear [illegible]

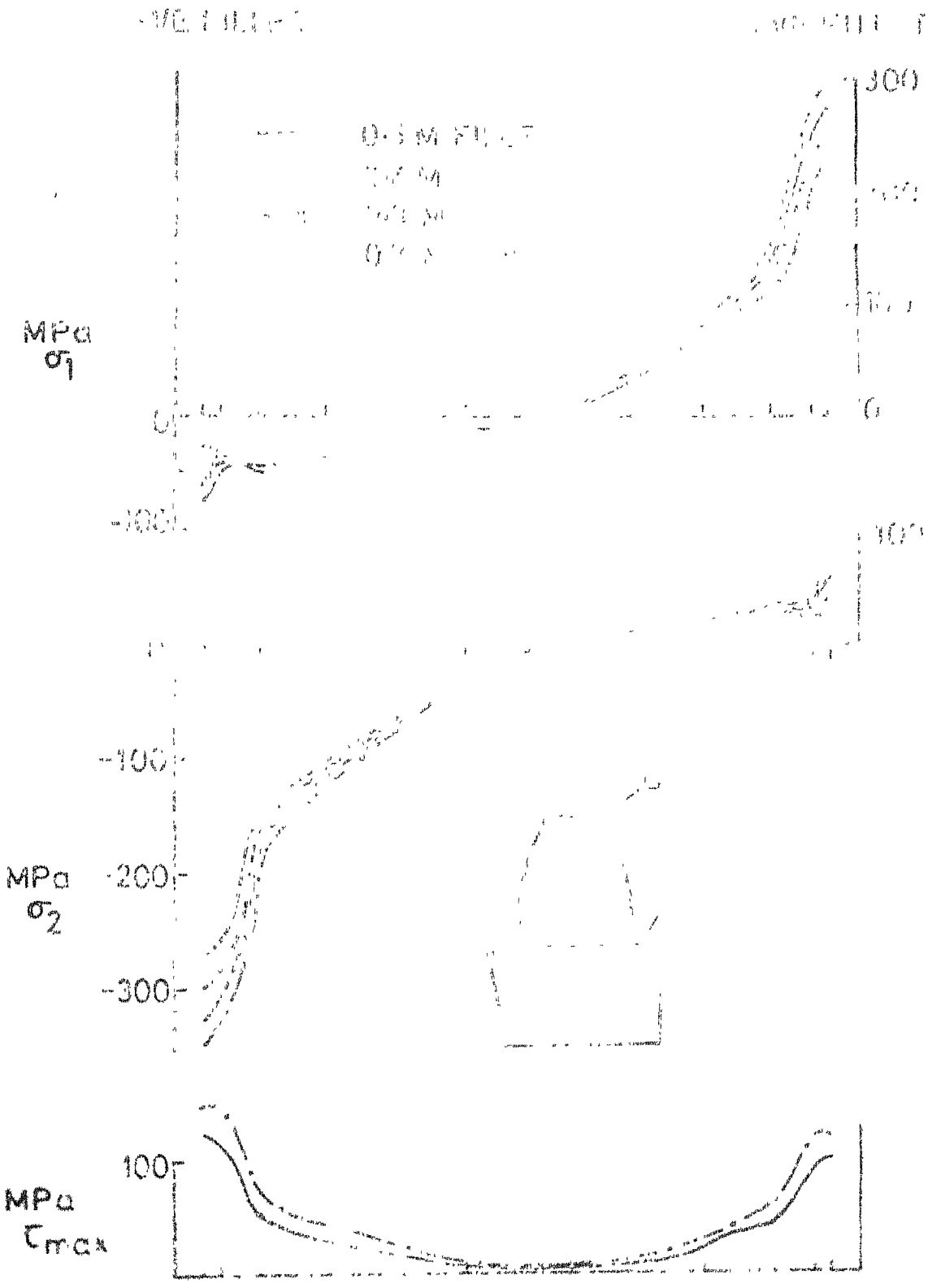

Fig.3-4 Stresses across [illegible] section of solid, SG 2[illegible]

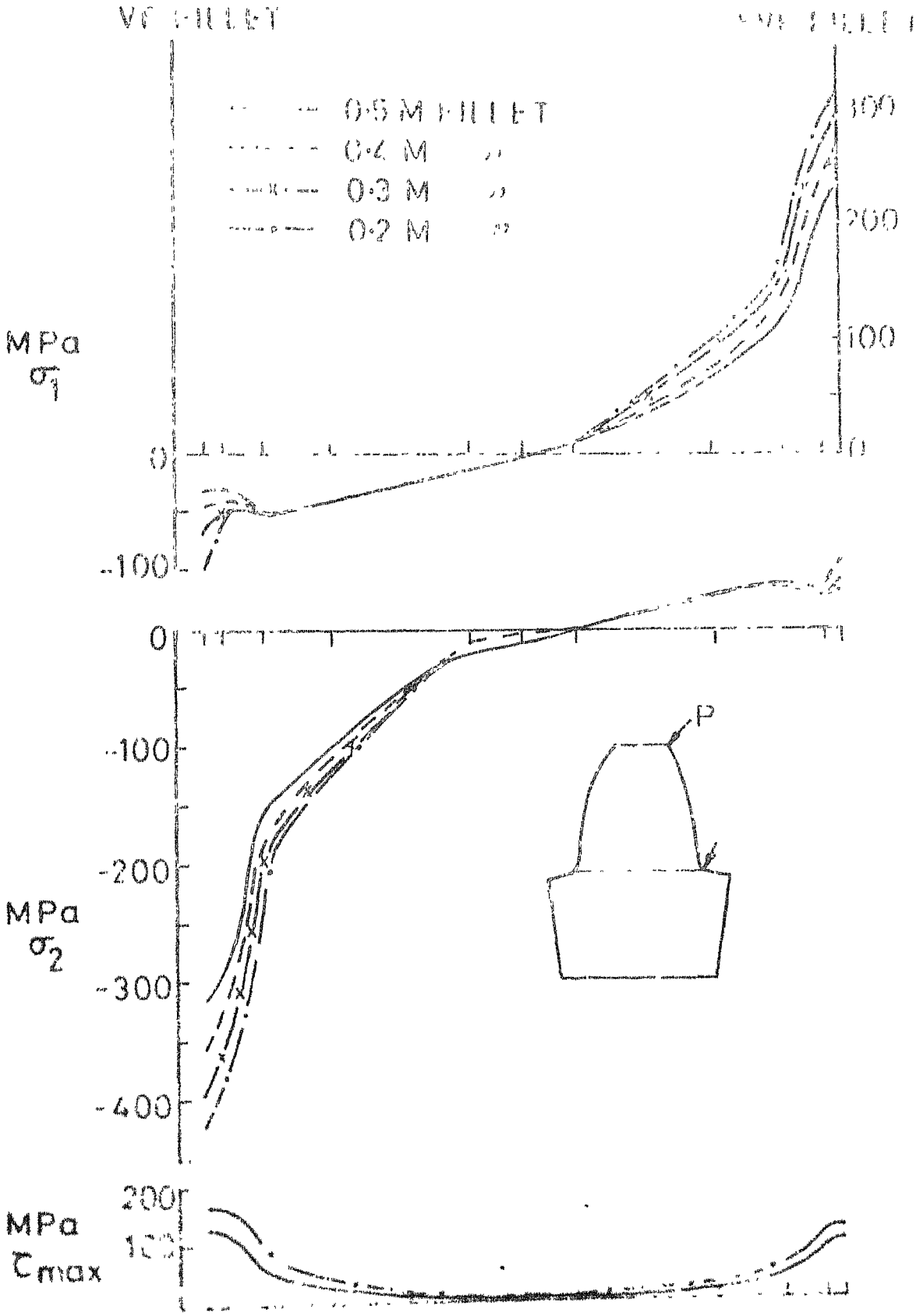

Fig.35 Stresses across the tooth section of rim gear SG 70 for different fillet radii

Fig.3·6(a) Stress along the curve fillet length

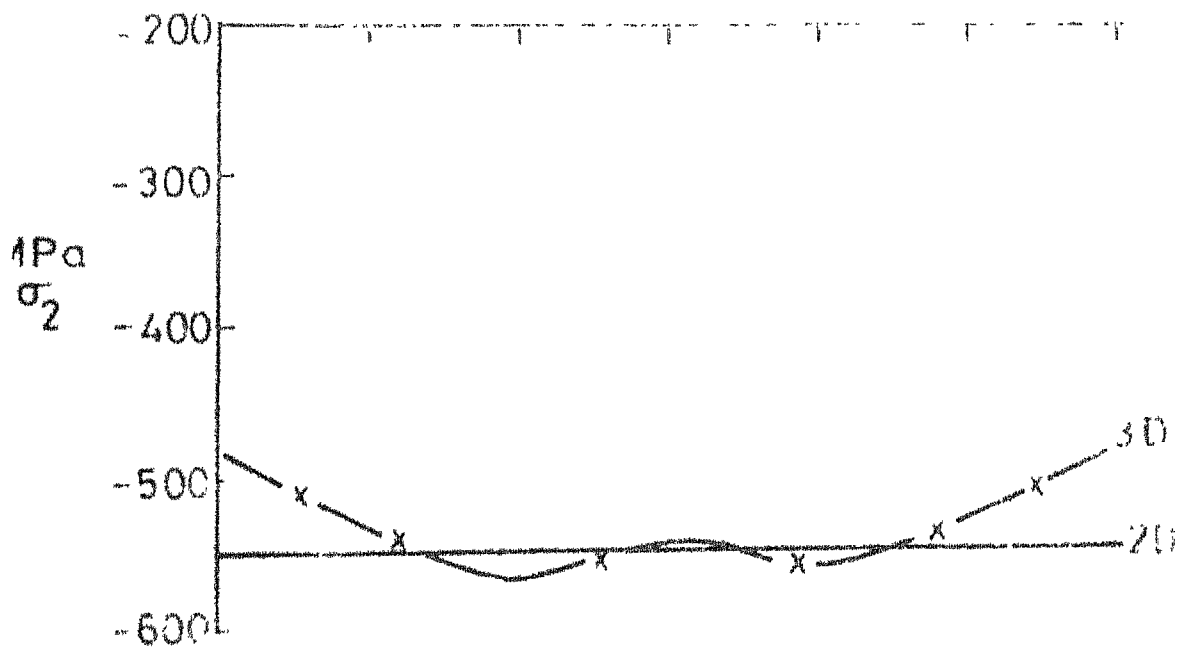

Fig.3·6(b) Stress along the curve fillet length.SG 90 as 3-D body

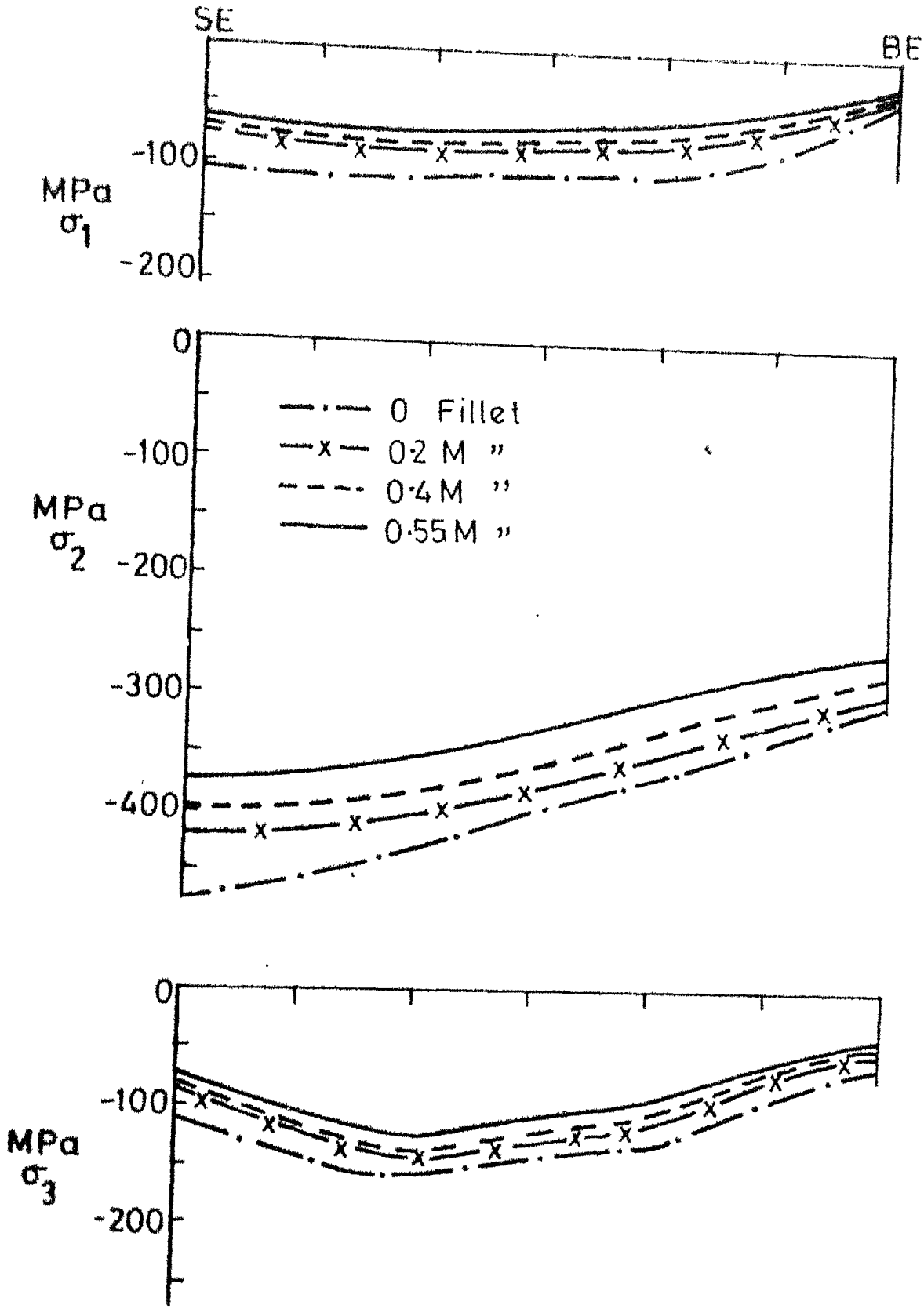

Fig. 3·7(a) Stresses along the -ve fillet length, BG 100

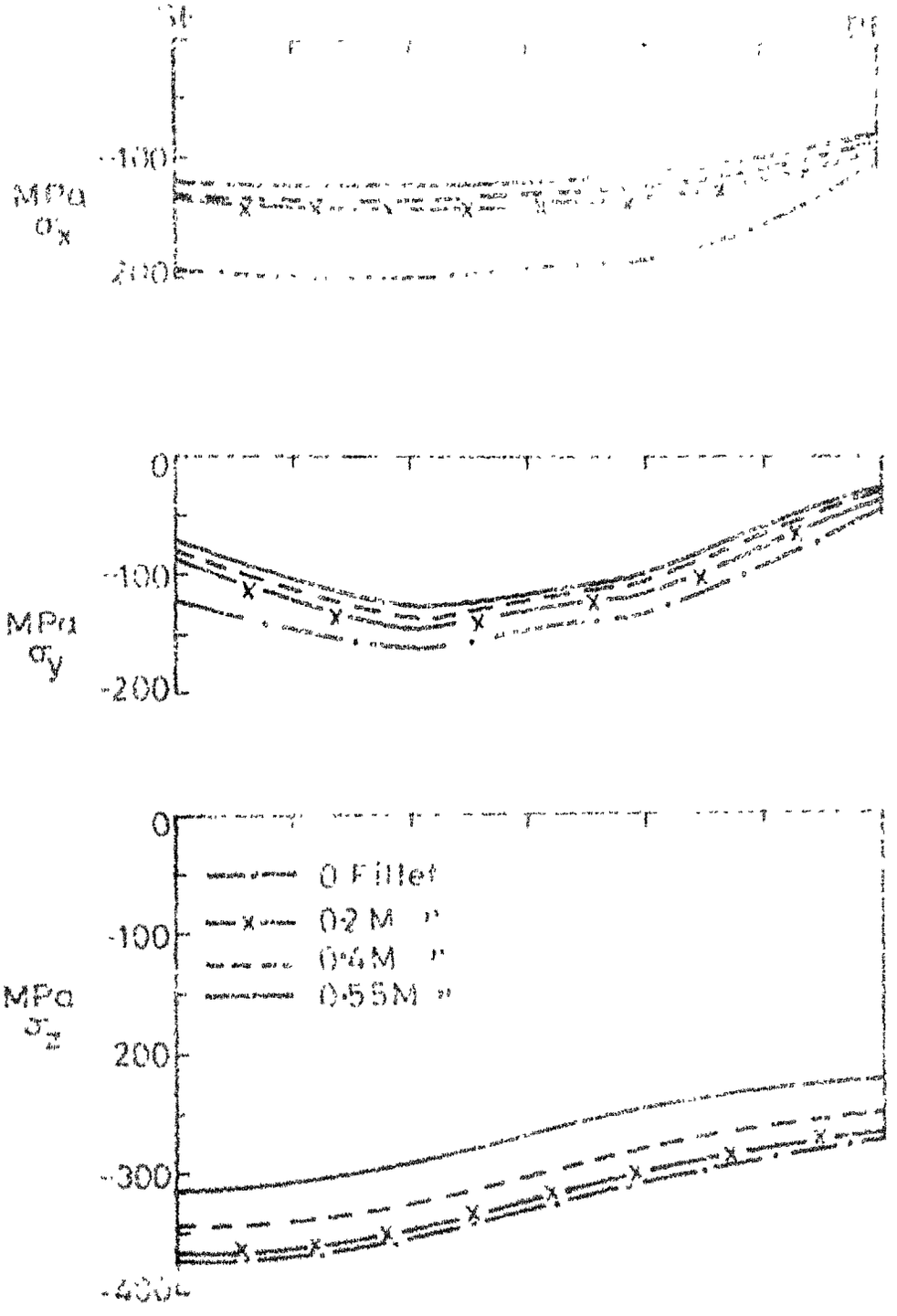

Fig.3.7(b) Stresses along the -ve fillet length, BG 100

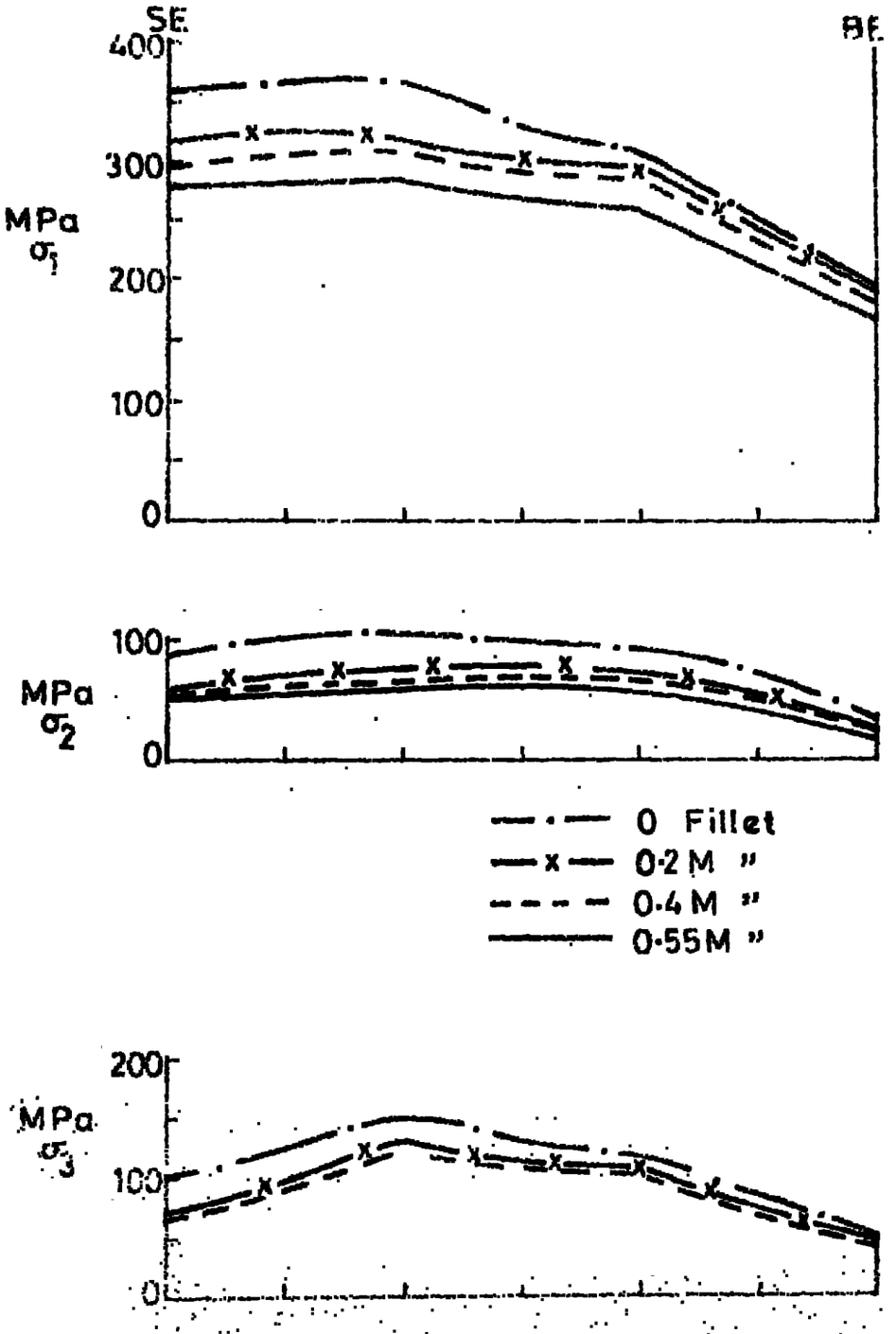

Fig 3.8 (a) Stresses along the +ve fillet length, BG 100

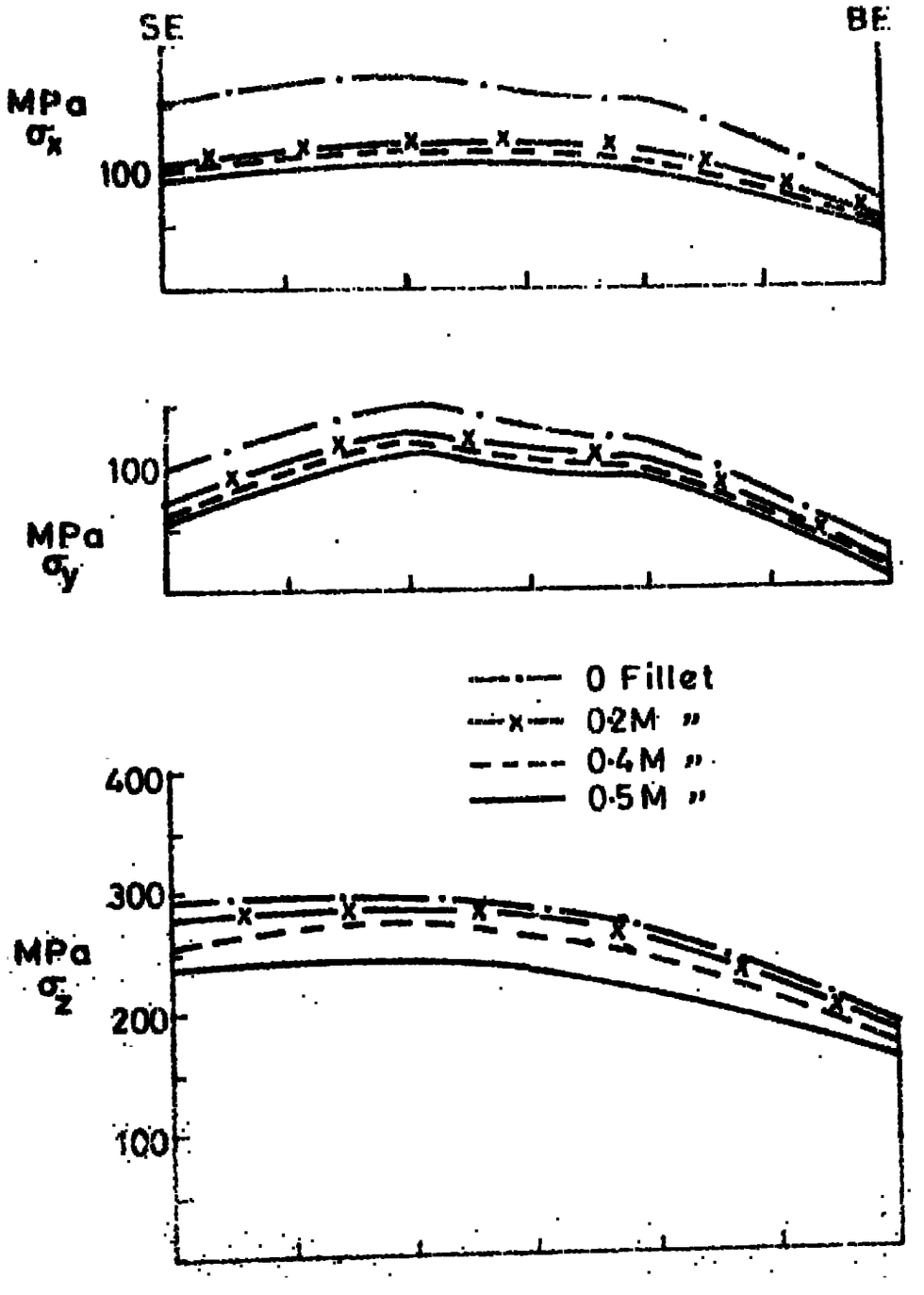

Fig 3.8(b) Stresses along the +ve fillet length, BG100

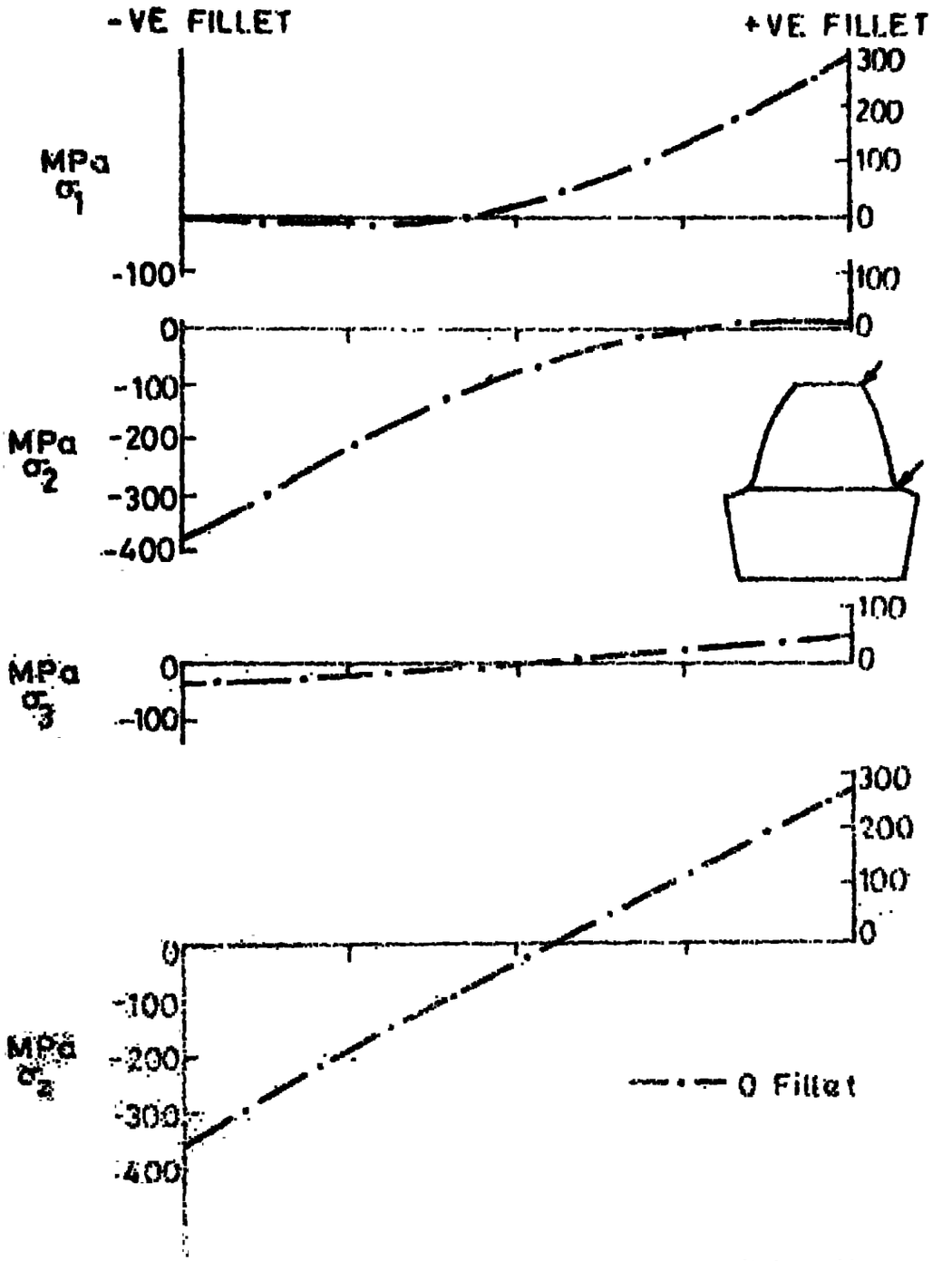

Fig 39 Stresses across the tooth section, shorter end, BG 100

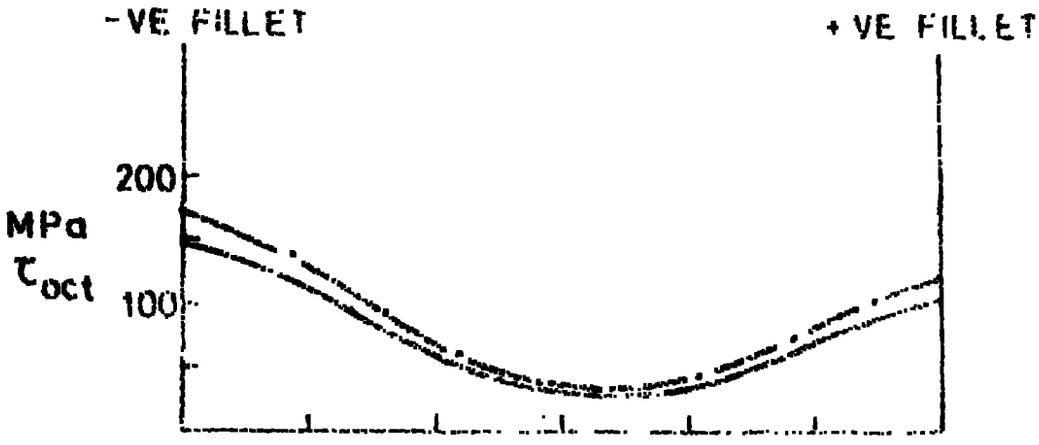

Fig.3-10 (a) Octahedral shear stress across the tooth section, BG 100

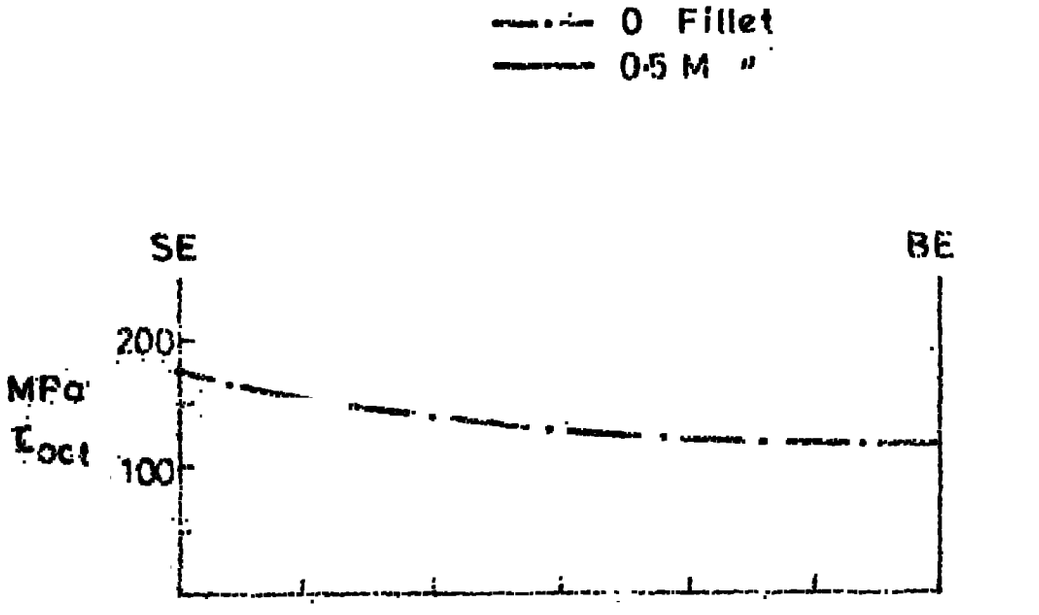

Fig.3-10(b) Octahedral shear stress along the length, BG 100

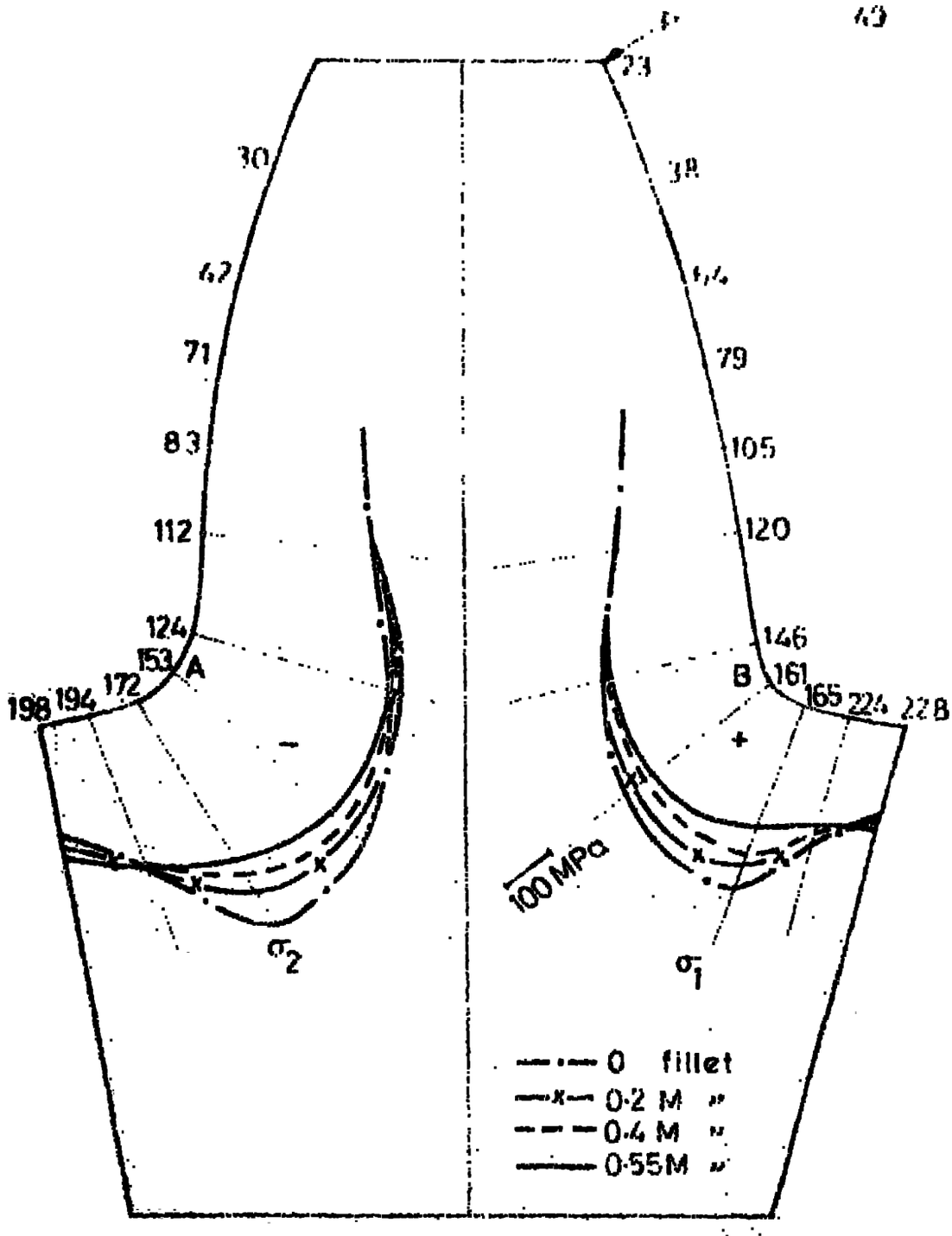

Fig.3.11 Stresses along the profile at shorter end, BG 100

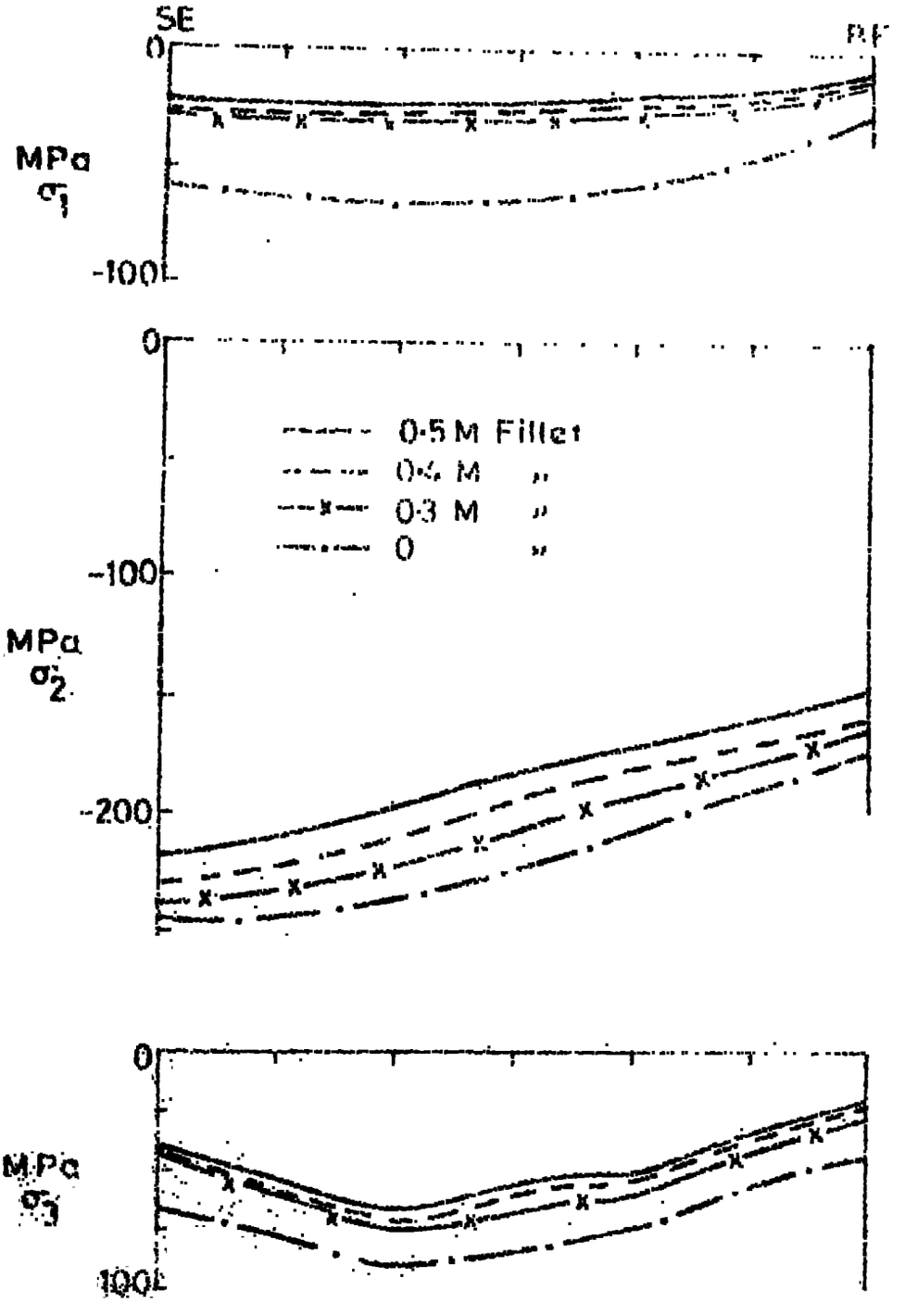

Fig 3.12 a) Stresses along the -ve fillet length

BG 180

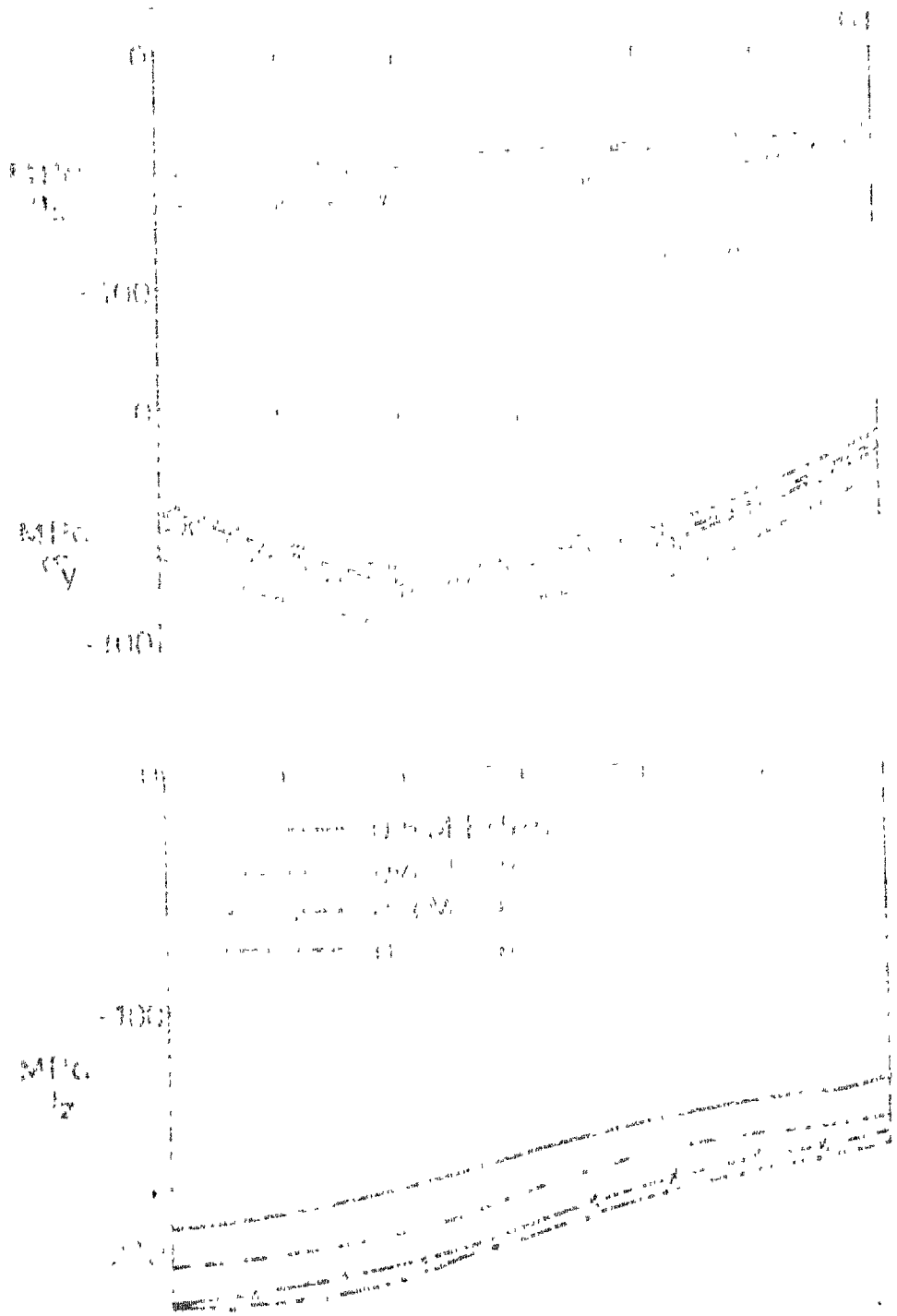

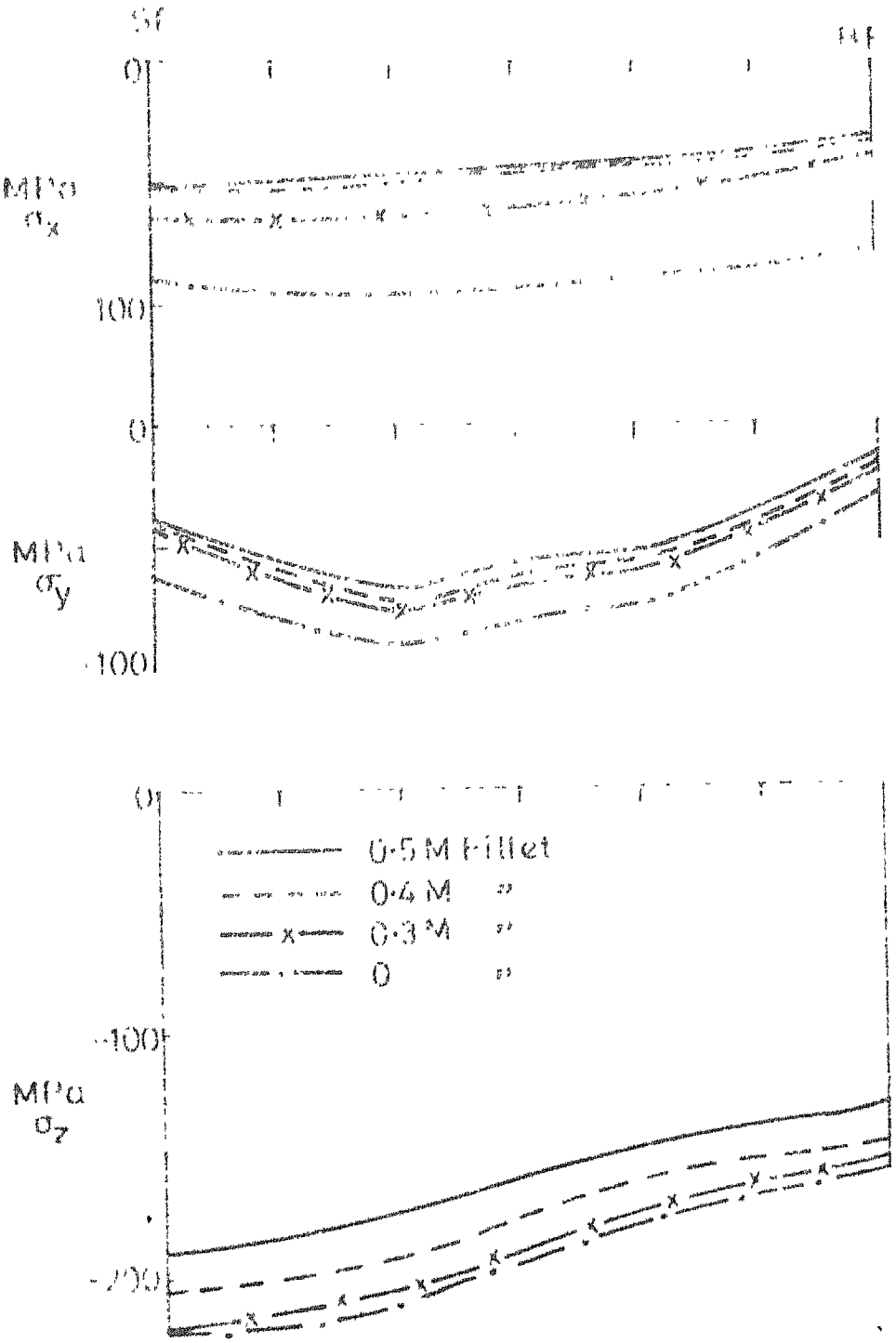

Fig 3·12 (b) Stresses along the -ve fillet length BG 180

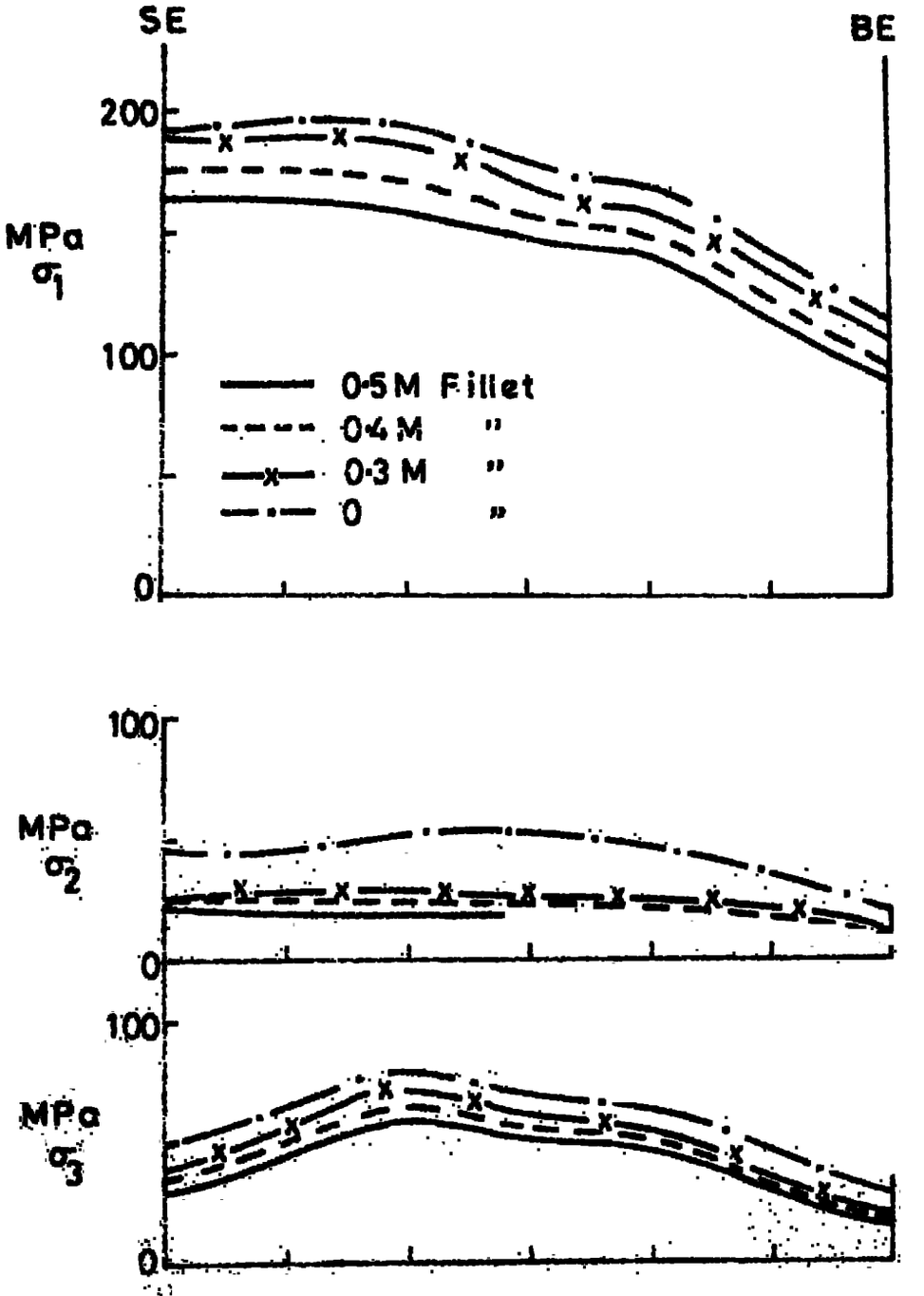

Fig 3.13(a) Stresses along the +ve fillet length BG 180

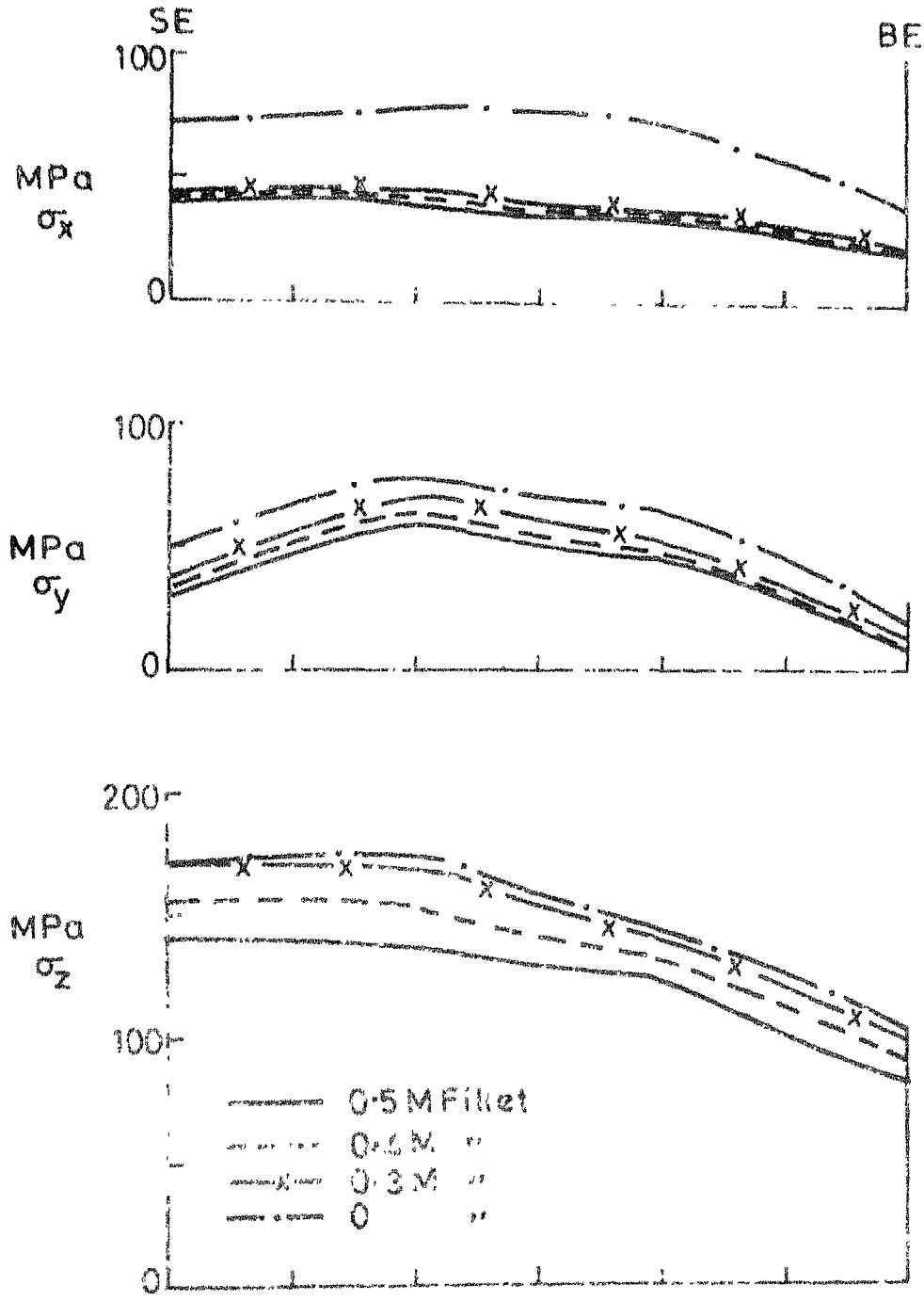

Fig.3·13(b) Stresses along the +ve fillet length, BG 180

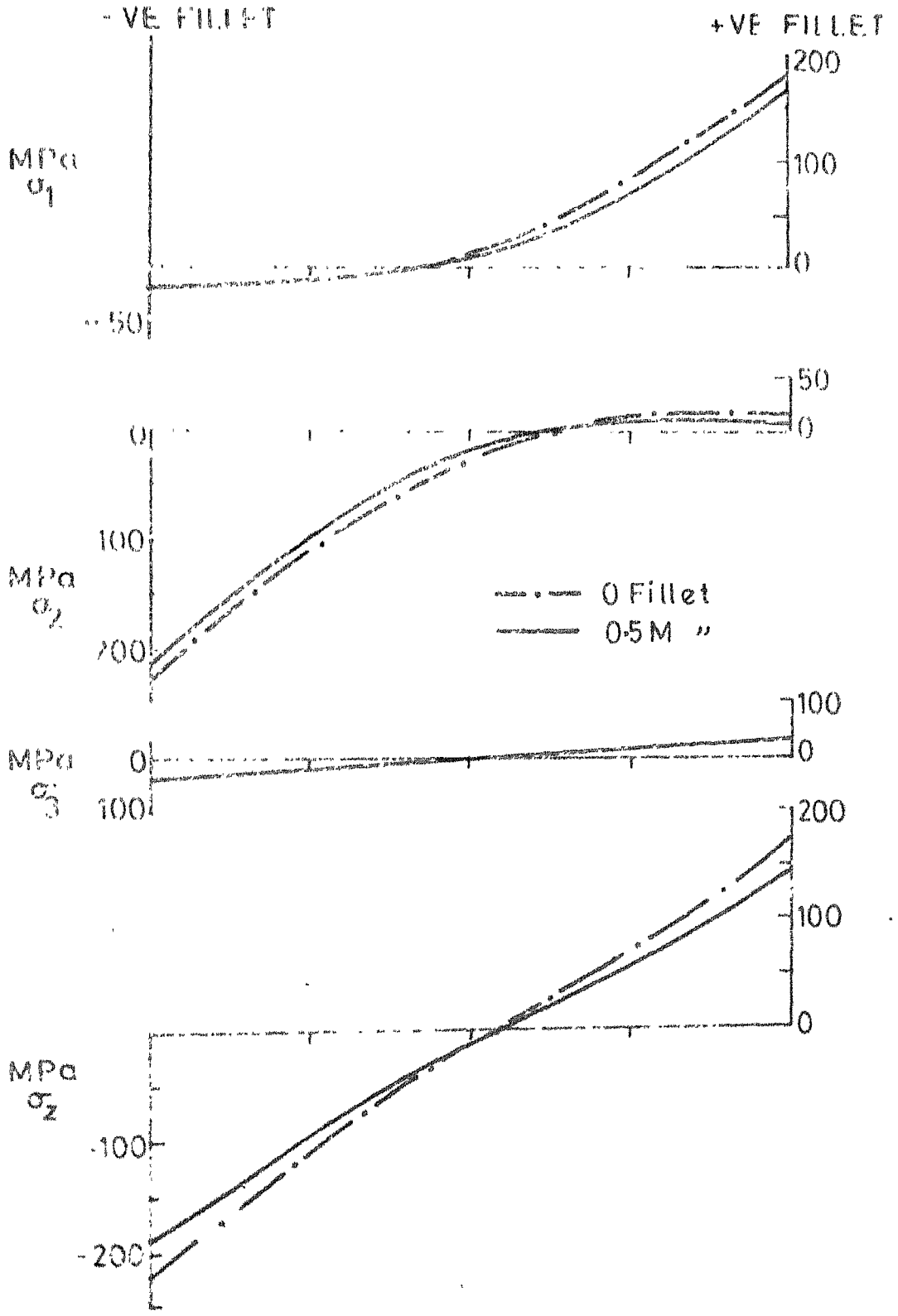

Fig.3·14 Stresses across the tooth section, BG 180

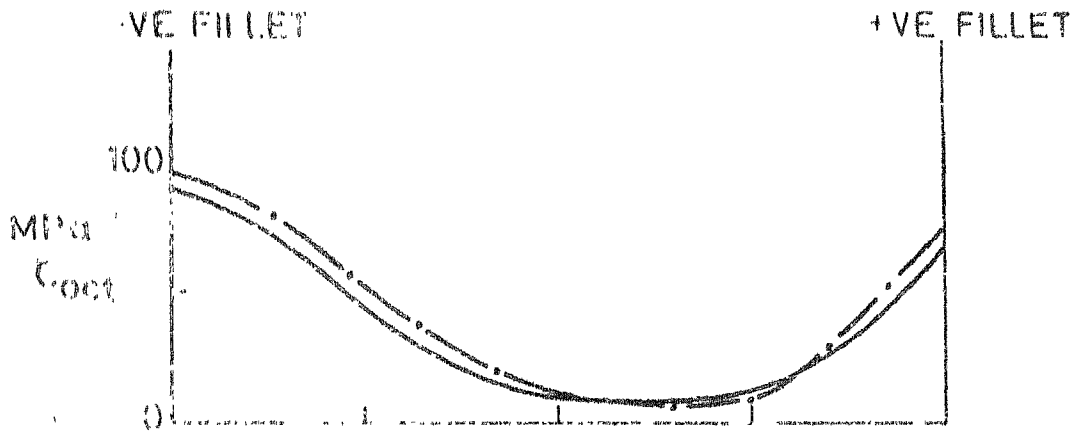

Fig.3.15 (a) Octahedral shear stress across the tooth thickness, BG 180

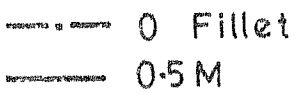

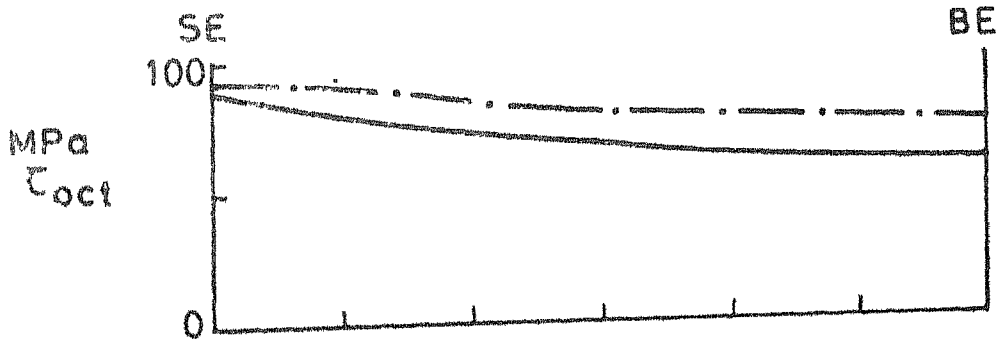

Fig.3.15 (b) Octahedral shear stress along the -ve fillet length, BG 180

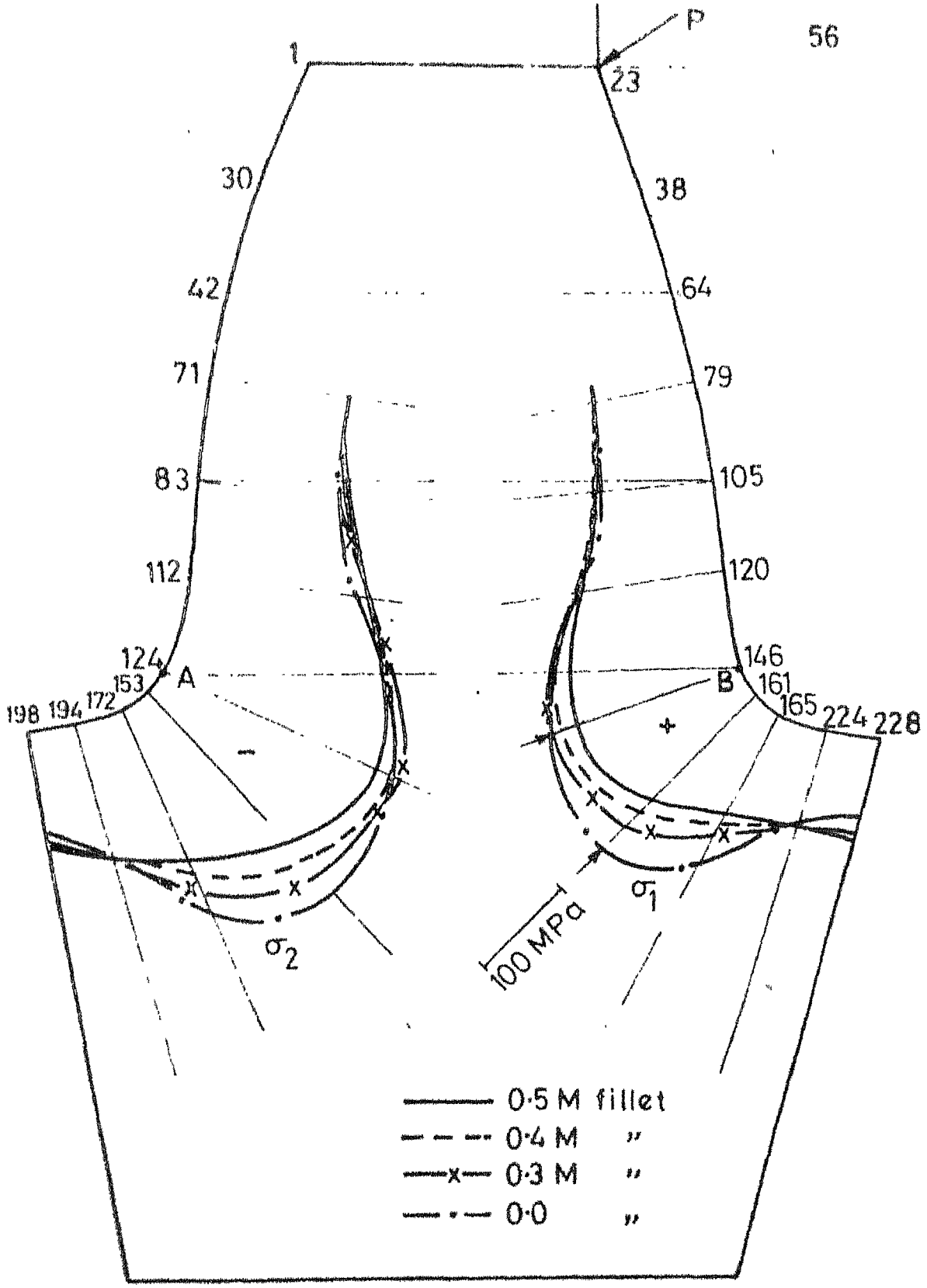

Fig.3·16 Stresses along the profile at shorter end, BG 180